

## Research Article

# Impacts of BaO additives on the mechanical, optical and radiation shielding properties of BaO–K<sub>2</sub>O–CoO–Al<sub>2</sub>O<sub>3</sub>–B<sub>2</sub>O<sub>3</sub> glasses

A. Samir<sup>a</sup>, Moukhtar A. Hassan<sup>b,\*</sup>, F. Ahmad<sup>c</sup>, M.S. Sadeq<sup>d,e,\*\*</sup>, S.Y. Marzouk<sup>f</sup>, H. Y. Morshidy<sup>d,g,\*\*\*</sup>

<sup>a</sup> Basic Science Department, Faculty of Engineering at Shoubra, Benha University, 11629, Egypt

<sup>b</sup> Physics Department, Faculty of Science, Al-Azhar University, 11884, Cairo, Egypt

<sup>c</sup> Physics Department, Faculty of Science, Al-Azhar University (Girls Branch), 11754, Cairo, Egypt

<sup>d</sup> Basic Science Department, Faculty of Engineering, Sinai University, Egypt

<sup>e</sup> MEU Research Unit, Middle East University, Amman, Jordan

<sup>f</sup> Arab Academy of Science and Technology, 2033, Al-Horria, Heliopolis, Cairo, Egypt

<sup>g</sup> Research & Studies Center, Midocean University, Moroni, 6063, Comoros

## ARTICLE INFO

## Keywords:

Co<sup>2+</sup> and

Ba<sup>2+</sup> ions

Mechanical properties

Shielding purposes

## ABSTRACT

This article reports the influence of barium oxide (BaO) on mechanical and radiation protection characteristics of BaO–K<sub>2</sub>O–CoO–Al<sub>2</sub>O<sub>3</sub>–B<sub>2</sub>O<sub>3</sub> glass. The obtained results confirmed the enhanced the elastic moduli, confirming a high cross-linked density, high impact resistance, and toughness of the network, with the good mechanical stability of samples with further additives of BaO. In detail, with increasing BaO contents, it is observed that the shear modulus increased from 33.8 GPa reaching 37.7 GPa (increased by about 11.5%), while the longitudinal modulus enhanced from 100.5 GPa up to 117.4 GPa (enhanced by ~ 16.8%), besides Young's modulus augmented from 84.4 GPa to 95.3 GPa (augmented by ~ 13%), and bulk modulus is increased from 55.4 GPa reaching 67.2 GPa (increased by ~ 21.3%). These enhancements in the elastic moduli are attributed to the increased tetrahedral units (BO<sub>4</sub> and AlO<sub>4</sub> units) inside the glass matrix with increasing BaO additives. On the other hand, with increasing BaO, optical band gaps increase from 3.07 eV to 3.58 eV, and ligand field strength values decrease from 3494 cm<sup>-1</sup> to 3273 cm<sup>-1</sup>. Furthermore, the addition of BaO reduces the linear and nonlinear refractive indices. Moreover, the obtained radiation shielding parameters were studied and compared to those of well-known shielding materials. The comparison confirmed that the glass specimen with the highest barium oxide content has better radiation shielding ability than others and is suitable for radiation shielding applications.

## 1. Introduction

Radiation shielding concept is one of the most widely preventive ways against the scathes of high energy radiations [1]. On the application side, ionizing radiations are increasingly being used in industrial settings for topics like generating power, food sterilization, and related procedures. In addition to these advantageous circumstances, there is also another issue to take into account: protecting against the damaging effects of ionizing radiations sources. When interacting with live biological tissues, ionizing radiations may result in damage ranging from

tissue to cell, depending on their intensities and kinds of these radiations. Consequently, it is crucial to utilize adequate shields to inhibit interplay between harmful ionizing radiation sources and living tissue [2,3]. To lower the radiation dose from external exposure, different parameter should be considered. These parameters include: reduced exposure duration in the radiation field, increased separation from the source, and the use of a shield. Due to experimental constraints, reducing exposure duration can occasionally be challenging, but remote operation calls for sophisticated instrumentation to track the process. The most effective method is to utilize an absorber, which will lower the

\* Corresponding Author.

\*\* Corresponding author. Basic Science Department, Faculty of Engineering, Sinai University, Egypt

\*\*\* Corresponding author. Basic Science Department, Faculty of Engineering, Sinai University, Egypt

E-mail addresses: [m.a.hassan@azhar.edu.eg](mailto:m.a.hassan@azhar.edu.eg) (M.A. Hassan), [mhmd\\_sa3d@hotmail.com](mailto:mhmd_sa3d@hotmail.com) (M.S. Sadeq), [hesham\\_yahia25@yahoo.com](mailto:hesham_yahia25@yahoo.com) (H.Y. Morshidy).

radiation's intensity and, as a result, the effective dose. Depending on the radiation type, energy, and temperature of the area around the source, as well as taking space and cost into consideration, different types of shielding materials are utilized [4]. Several studies including both theoretical and experimental techniques have been attempted to assess the radiations attenuation capabilities of various shielding materials such as radiation shielding glasses [5–11].

The addition of several modifier cations such as alkali and alkaline cations were observed to enhance the glass stability and homogeneity [12]. The barium oxide (BaO) is one of alkaline earth oxide. Barium ions have distinct role in shielding properties due to their physical features including high atomic radius, high transparency, and high mass-density compounds. Barium oxide is suitable for utilization at wide energy windows such as x-ray and gamma-ray [13,14].

Recently, several studies were reported on the significance of shielding against harmful radiation. N. K. Libeesh et al. [15] studied the radiation shielding properties of the rock types, along with the remote sensing aspects using the image processing technique. While P. E. Teresa et al. [16] used the classical melt-quenching method to add some of modifiers to alkali borotellerate glasses. We used the same method to prepare our samples. Moreover, M. A. Imheidat et al. [17] studied the radiation shielding, mechanical, optical, and structural properties for tellurite glass samples doped with 20 mol % of barium oxide. They evaluated all mechanical features such as dissociation energy per unit volume, packing density, Young (E), Bulk (B), Shear (S), and Longitudinal (L) modulus. Simultaneously, the radiation shielding properties were assessed experimentally within the energy range from 0.184 to 0.810 MeV.

Moreover, several studies reported effective attempts to assess the radiations attenuation capabilities of various shielding materials such as radiation shielding glasses including barium oxide. Zakaly et al. [14] have studied the role of barium oxide on shielding features of alumino-borate glasses network. They compared the obtained experimental results with theoretical ones of shielding coefficients such as MAC, LAC, HVL, and TVL. Moreover, Mhareb et al. [18] have studied the role of barium oxide on physicochemical and shielding properties of sodium zinc borate glasses. Using Phy-X program, their results indicate that the best performance in shielding protection were obtained for high-density sample (Ba-30). Furthermore, Aloraini et al. [19] have studied the impact of barium oxide on shielding competence of glass material. The linear attenuation coefficient (LAC) of these glasses is reached maximum for 20 mol % of BaO, between 0.0395 MeV and 0.411 MeV, while the effective atomic number of 10 mol % of BaO was equal to 36.66 at 0.0395 MeV. They conclude that the further addition of BaO content exhibits more desirable radiation protection characteristics. Overall, according to the previously reported works [20–22], glass materials grant distinguished properties for shielding against harmful radiations compared to other materials. In addition, the obtained properties of heavy-weight barium-based borate glasses were compared to those obtained in the recent glass materials reported in Refs. [23–25].

Harsh glasses including the mechanical properties of being “hard” and “crack-resistant” are demand in many high technological advanced applications such as construction, means of transportation, and electronics [26]. Furthermore, the high mechanical strengths of shielded glasses are required; therefore, some precautions should be considered for these glasses. The investigation of mechanical characteristic is a suitable technique that was exploited to evaluate the elastic features of the studied glass system. However, the well-known innate fragility of glass material restricts its utility in modern applications. The realization seeking of best hardness and harsh resistance of cracks has been a topic of interest for researcher in glass science. It is established that Vickers hardness (HV) is exploited to determine the hardness of glass material [26]. In oxide glasses, Vickers hardness can be induced through the compositional and structural parameters. Yamane et al. proposed a relation, for silicate glasses, in which HV is proportional to the square root of the product between the bulk modulus  $K$ , shear modulus  $G$ , and

the average single-bond energy between the constituent component cations and oxygen anions [27]. Regarding the relation between Vickers hardness and Young's modulus ( $E$ ), positive linear tendencies have been obtained [28,29]. According to the Makishima and Mackenzie model, the elastic moduli including Young's modulus  $E$ , bulk modulus  $K$ , and shear modulus  $G$  of glass material are related to both the energy of dissociation per unit volume of the constituent components and the calculated atomic packing density [30,31]. In case of silicate glasses including alkali-alkaline earth metal oxides, it was reported that such glasses with more packed structures had higher values of both hardness and elastic moduli [32]. The impactful role of barium oxide on the elastic parameters in glasses was evaluated by Bhattachary and Shashikala [33].

In this regard, we investigated the role of barium oxide addition (0–20 mol %) on mechanical and radiation shielding competence. The distinguished mechanical-shielding relationship of heavy-weight barium-based borate glasses paved the route toward the applicability of our samples in radiation shielding application.

## 2. Experimental methodology

Cobalt-alumino-borate glass system with the following composition were successfully prepared using the traditional melt quenching method; [x BaO – (20-x) K<sub>2</sub>O 63.5 B<sub>2</sub>O<sub>3</sub> – 15 Al<sub>2</sub>O<sub>3</sub> – 1.5 CoO]. Barium oxide was loaded at the expense of potassium oxide with content from 0 mol % reaching 20 mol %. Raw materials of H<sub>3</sub> B O<sub>3</sub>, K<sub>2</sub> C O<sub>3</sub>, CoO, BaCO<sub>3</sub> and Al<sub>2</sub>O<sub>3</sub>, with high purity, were utilized as starting ingredients. These substances are weighed in accordance with their mol. % by an electronic balance with a 0.001 g accuracy, then they ground in an agate mortar until a uniform mixture is achieved. Thereafter, the powder put into crucibles, which made from porcelain, in a furnace to carbonize at 600 °C for 30 min then increasing the temperature at 600 °C for 45 min. The melting process occurred at [1100 °C–1180 °C], depending on chemical composition. The resulting molten was carefully stirred to ensure some homogeneity of samples. Finally, the resulting molten was poured and quenched at room temperature between two smoothed copper plates. The obtained specimens at the end of preparation were brilliant, bubble-free, and hard.

The ultrasonic wave velocities (shear and longitudinal), at room temperature, were measured using X-cut and Y-cut transducers (KARL-DEUTSCH, Germany). The operating frequency was 4 MHz. A digital detector of ultrasonic flaw type of (Krauthramer USIP 20, Germany) were utilized in this method.

## 3. Theoretical backgrounds

### 3.1. Radiation shielding parameters

Generally, the linear attenuation coefficient (LAC) is an important factor for measuring any material's shielding effectiveness. The LAC is a constant that describes the portion of decreased assigned photons on a material with unit thickness.

The formula that follows can be used to calculate this coefficient:

$$LAC = \frac{1}{d} \ln \frac{N_0}{N} \quad (1)$$

Where the  $N_0$  and  $N$  are the intensity of incidental and transmitted photons and  $d$  is the thickness of the medium. The unit of LAC is cm<sup>-1</sup> or mm<sup>-1</sup>.

The LAC is affected by the atomic number of the medium and its density. Also, it is an energy-dependent parameter. If we divided the LAC by the density of the medium, then we get the mass attenuation coefficient, namely:

$$MAC = \frac{1}{d \times \rho} \ln \frac{N_0}{N} \quad (2)$$

**Table 1**

Measured values of both longitudinal ( $V_l$ ) and shear ( $V_s$ ) ultrasonic wave velocities, shear modulus (S), longitudinal modulus(L), Young's modulus (E), bulk modulus (K), and Poisson's ratio  $\sigma_p$ ), microhardness ( $H_\mu$ ), mean sound velocity ( $V_{mean}$ ), Debye temperature ( $\theta_D$ ), and softening temperature ( $T_s$ ) of all glass samples.

Sample (mol. %)	$V_l$ (m/s) $\pm 2$	$V_s$ (m/s) $\pm 2$	S (GPa) $\pm 10$ Pa	L (GPa) $\pm 10$ Pa	E (GPa) $\pm 10$ Pa	K (GPa) $\pm 10$ Pa	$\sigma_p$	$H_\mu$ (Kg/m <sup>2</sup> ) $\pm 0.001$	$V_{mean}$ (m/s) $\pm 2$	$\theta_D$ (K) $\pm 2$	$T_s$ (K) $\pm 2$
0 Ba	6886	3996	33.8	100.5	84.4	55.4	0.246	5.729	4434	552	1082
5 Ba	6794	3905	35.1	106.3	88.0	59.5	0.253	5.771	4337	546	1083
10 Ba	6679	3824	35.9	109.4	90.1	61.6	0.256	5.833	4248	538	1089
15 Ba	6586	3742	37.0	114.7	93.4	65.3	0.262	5.882	4160	532	1091
20 Ba	6474	3669	37.7	117.4	95.3	67.2	0.263	5.948	4080	524	1096

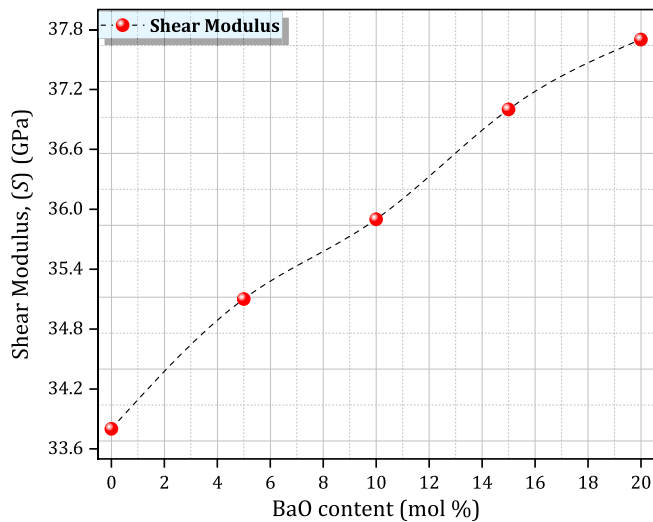


**Fig. 1.** Variations of shear modulus (S) versus BaO contents for KAlCoBBaO-glass samples.

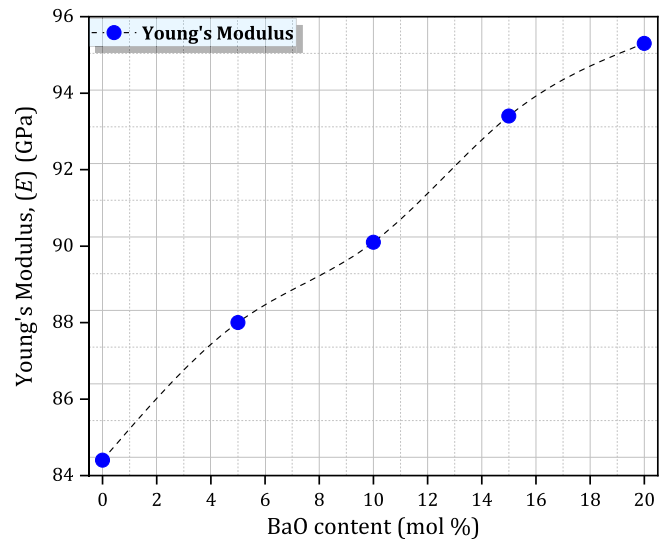


**Fig. 3.** Variations of Young's modulus (E) versus BaO contents for KAlCoBBaO-glass samples.

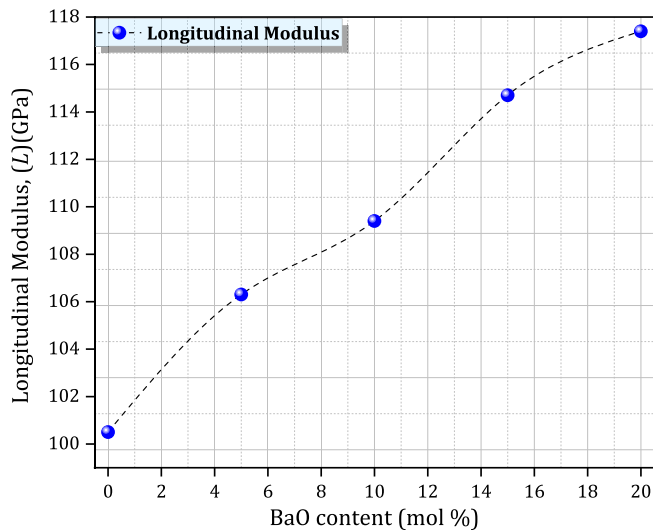


**Fig. 2.** Variations of Longitudinal modulus (L) versus BaO contents for KAlCoBBaO-glass samples.

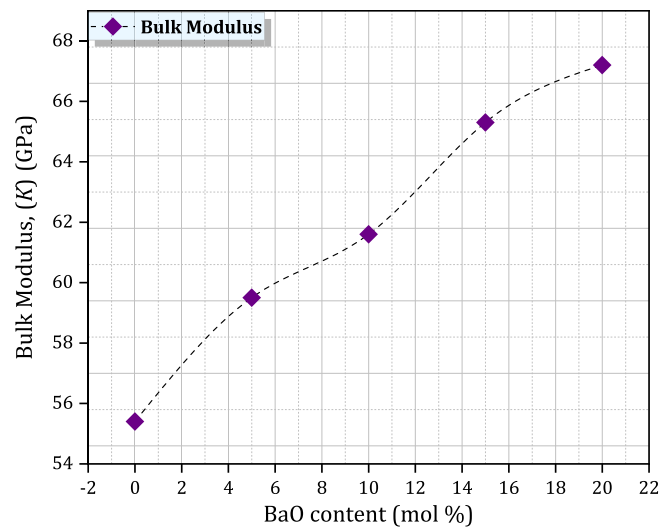


**Fig. 4.** Variations of Bulk modulus (E) versus BaO contents for KAlCoBBaO-glass samples.

In the aforementioned equation,  $\rho$  is the density of the medium.

Half value of layer (HVL) refers to the specified absorbing material thickness that can reduce the intensity of the incoming radiation in 50%. Numerically,

$$HVL = \frac{0.693}{LAC} \quad (3)$$

From the LAC, we can also derive the mean free path and TVL as:

$$MFP = \frac{1}{LAC} \quad (4)$$

$$TVL = \frac{2.3}{LAC} \quad (5)$$

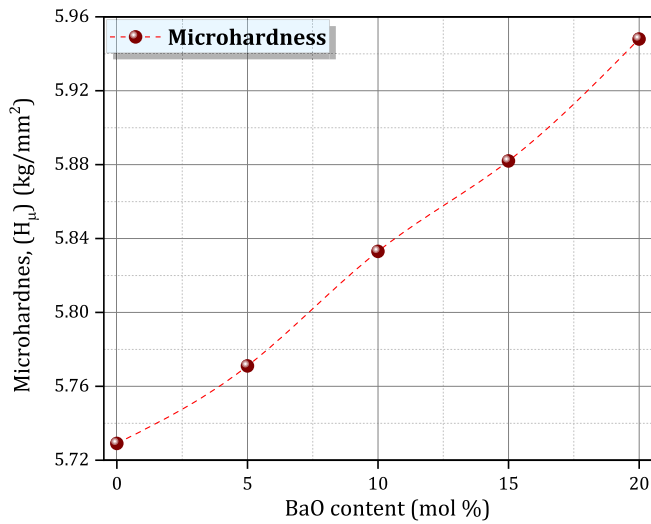


Fig. 5. Variations of Microhardness ( $H_{\mu}$ ) versus BaO contents for KAlCoBBaO-glass samples.

It is noting, to gain insights into the radiation shielding characteristics for the prepared glasses, we can use Phy-X software, which is a free online software and can derive different shielding parameters using a package software available online at <https://phy-x.net/PSD> [34].

### 3.2. Mechanical properties

The ultrasonic pulse-echo method is suitable technique that was exploited to gain insights into the elastic features of the studied glass system. Specifically, the ultrasonic velocities were measured using the well-known relation:  $V = 2x/\Delta t$ , where  $x$  is the thickness of samples and  $\Delta t$  is time interval. The measured values of both longitudinal ( $V_l$ ) and shear ( $V_s$ ) ultrasonic wave velocities. Moreover, the determination of elastic properties, such as shear modulus ( $S$ ), longitudinal modulus ( $L$ ), Young's modulus ( $E$ ), bulk modulus ( $K$ ), and Poisson's ratio ( $\sigma_p$ ), is an essential issue in understanding the structural-mechanical relationships of the studied glasses. To understand the nature of these moduli, it is well-known that the elasticity, in general, is the ability of a material to resist the deformation when an exerted force is applied on it and returns to its pristine shape when such force is omitted. Glass is one of material that undergoes three important types of stress (i.e., stress) such as uniaxial, triaxial stresses, and free or pure stress. Strain is due to these stresses [35].

Shear modulus ( $S$ ) is the ratio of the triaxial stress to the resulting strain, and could be determined from the relation [36,37]:

$$S = \rho V_s^2 \quad (6)$$

while the longitudinal modulus ( $L$ ) is determined by the following relation [36,37]:

$$L = \rho V_l^2 \quad (7)$$

where  $\rho$  is the samples' density.

Young's modulus ( $E$ ), as one of such important elastic moduli, is the ration of uniaxial stress to the formed strain in the glass sample, and is determined through the following relation [36,37]:

$$E = S \left[ \frac{3V_l^2 - 4V_s^2}{V_l^2 - V_s^2} \right] \quad (8)$$

Bulk modulus ( $K$ ) is the ratio of pure stress to the formed stain and is estimated from the following relation [35–37]:

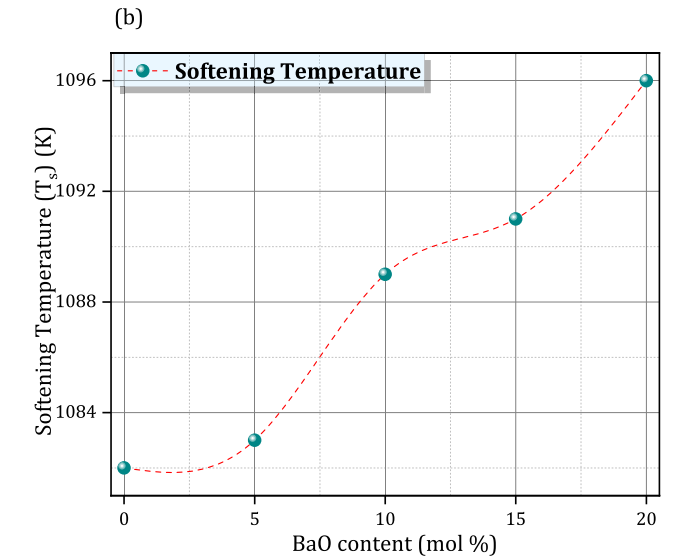
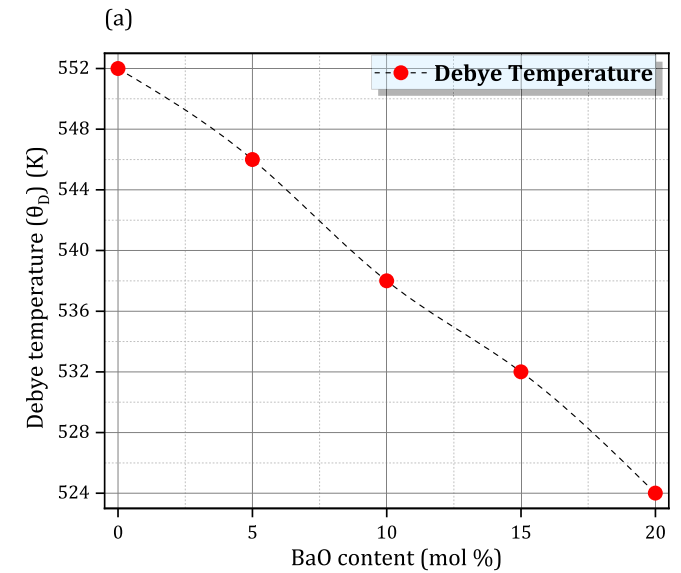


Fig. 6. (a and b): (a) Variations of Debye temperature ( $\theta_D$ ) and (b) softening temperature ( versus BaO contents for KAlCoBBaO-glass samples.

$$K = L - \left[ \frac{4S}{3} \right] \quad (9)$$

Poisson's ratio is well-known that it is the ratio between the lateral to axial strain of the material. It is calculated using the relation [35–37]:

$$\sigma_p = \left[ \frac{\text{Lateral Strain}}{\text{axial Strain}} \right] \quad (10)$$

Other additional informative parameters that describe the mechanical properties of material are microhardness, mean sound velocity, Debye temperature, and softening temperature.

Microhardness ( $H_{\mu}$ ) determines the ability of material to withstand friction and predicts some mechanical properties such as tensile strength and toughness. The microhardness can be determined from the following relation [35–37]:

$$H_{\mu} = \left[ 1 - \frac{V_l^2 - V_s^2}{V_l^2 + V_s^2} \right] \quad (11)$$

The mean sound velocity ( $V_{mean}$ ) is determined from the relation [36]:

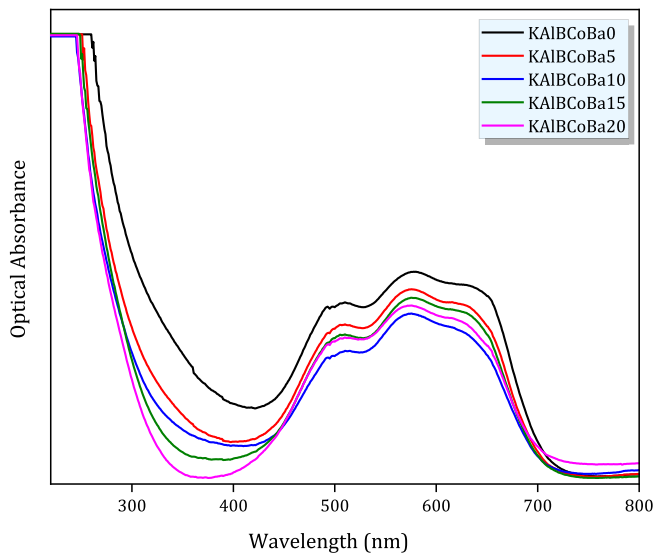


Fig. 7. The optical absorbance of KAlCoBa-glass samples within ultraviolet and visible regions.

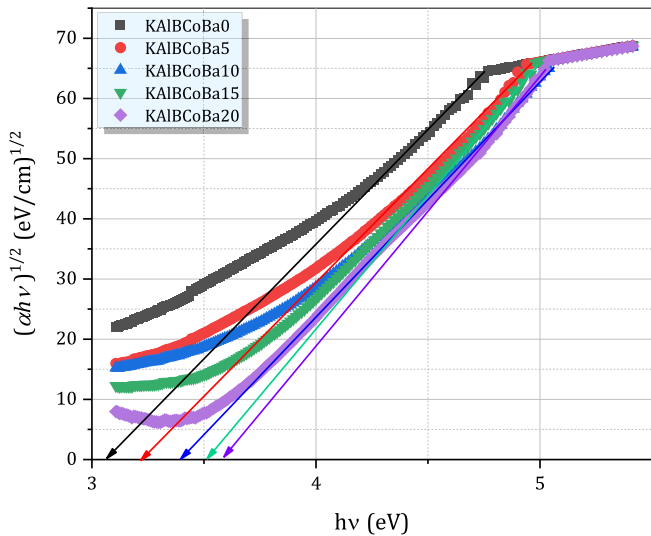


Fig. 8. plot of  $(\alpha hv)^{1/2}$  against  $h\nu$  (Tauc's plot) for the prepared KAlCoBa15-glass samples.

$$V_{mean} = \left[ \frac{1}{3} \left[ \frac{1}{V_I^3} + \frac{1}{V_S^3} \right] \right]^{-1/3} \quad (12)$$

Debye temperature ( $\theta_D$ ) is the temperature at which approximately all network vibrational modes are excited. Debye temperature is determined through the relation [36]:

$$\theta_D = V_{mean} \left[ \frac{h}{K_B} \right] \left[ \frac{3N_A \psi}{4ITV_m} \right]^{1/3} \quad (13)$$

where  $K_B$ ,  $N_A$ ,  $V_m$ , and  $\psi$  are Boltzmann constant, Avogadro number and number of atoms in the chemical composition, respectively.

Finally, softening temperatures ( $T_s$ ) is defined as the temperatures at which the flow converts from viscous to plastic type. It is determined from the relation [38]:

$$T_s = \left[ \frac{V_s M}{C^2 \psi} \right] \quad (14)$$

where M is the molecular weight and C is a factor has value of 507.4 m

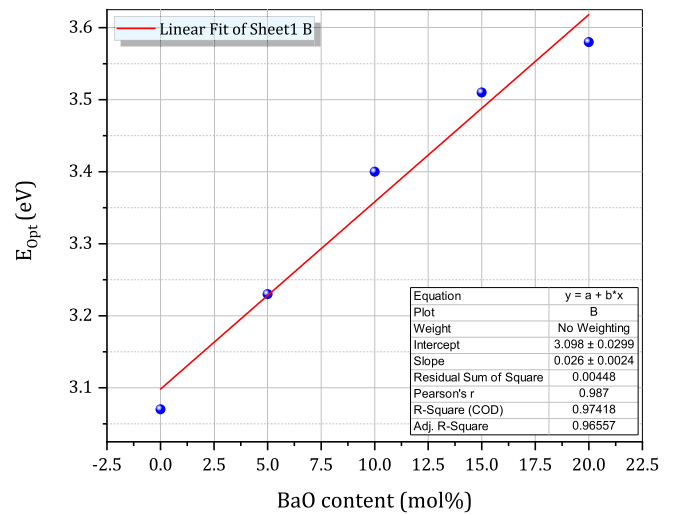


Fig. 9. The variations of optical band gap ( $E_{opt}$ ) versus BaO content for KAlCoBa15-glass samples.

Table 2

Optical band gap energy ( $E_{opt}$ ), Urbach energy ( $E_U$ ), metallization criterion ( $M$ ) and electron-phonon interaction ( $E_{e-p}$ ), of all glass samples.

Sample (mol. %)	$E_{opt}$ (eV)	$E_U$ (eV)	$M$	$E_{e-p}$ (eV)
0 Ba	3.07	1.06	0.392	27.69
5 Ba	3.23	0.85	0.402	22.24
10 Ba	3.4	0.67	0.412	17.35
15 Ba	3.51	0.45	0.419	11.78
20 Ba	3.58	0.37	0.423	9.60

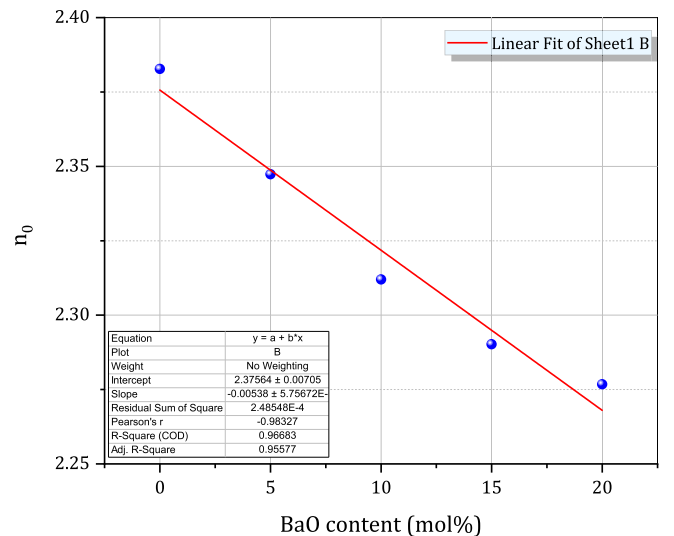


Fig. 10. The variations of refractive index ( $n_0$ ) versus BaO content for KAlCoBa15-glass samples.

$s^{-1} k^{-1}$ .

## 4. Results and discussion

### 4.1. Mechanical properties

The obtained values of shear, longitudinal, Young's and Bulk moduli, with their uncertainty values, were estimated and recorded in Table 1. Furthermore, the variations of the values of shear, longitudinal, Young's

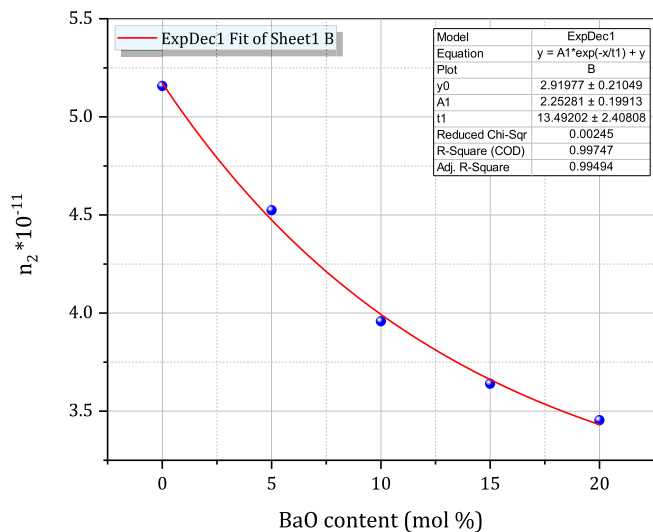


Fig. 11. The variations of nonlinear refractive index ( $n_2$ ) versus BaO content for KAlCoBa15-glass samples.

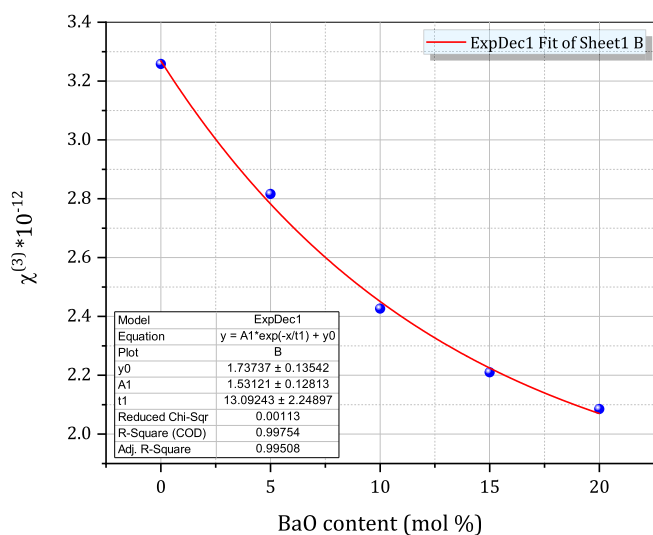


Fig. 12. The variations of third order nonlinear susceptibility ( $\chi^{(3)}$ ) versus BaO content for KAlCoBa15-glass samples.

and Bulk moduli against BaO contents are displayed in Figs. 1–4 respectively. Here, from the free-barium sample to the highest content of barium oxide here involved, it is observed that the shear modulus increased from 33.8 GPa reaching 37.7 GPa (increased to ~ 11.5%), while longitudinal modulus enhanced from 100.5 GPa up to 117.4 GPa (enhanced to ~ 16.8%), besides Young’s modulus augmented from 84.4 GPa to 95.3 GPa (augmented to ~ 13%), the last modulus is bulk that increased from 55.4 GPa reaching 67.2 GPa (increased to ~ 21.3%). This plausible augmentation in the elastic moduli is back to the introduced structural modifications when barium oxide was loaded instead of potassium oxide from 0 mol % to 20 mol %. There are more factors caused this observed increase such as the creation of  $BO_4$  and  $AlO_4$  units in the network. Other factor is the increase in bond strength, where the strength of Ba–O (84 kJ/mol) is larger than that of K–O (50 kJ/mol), (i.e., the dissociation energy of BaO is larger than that of  $K_2O$ ). Furthermore, the increased cross-link density reflects high connectivity, causes more increasing in the elastic properties of the prepared glassy specimens [36,37]. It is noted that the values of Poisson’s ratios are increased in the range (0.246–0.263) (increased to ~ 7%) with increasing the barium oxide content. It is observed that all values of

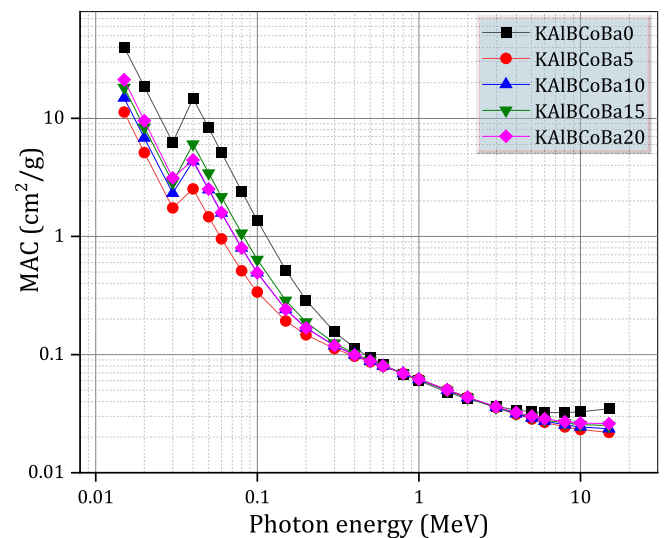


Fig. 13. The mass attenuation coefficient (MAC) as a function of the energy for KAlCoBa-glasses.

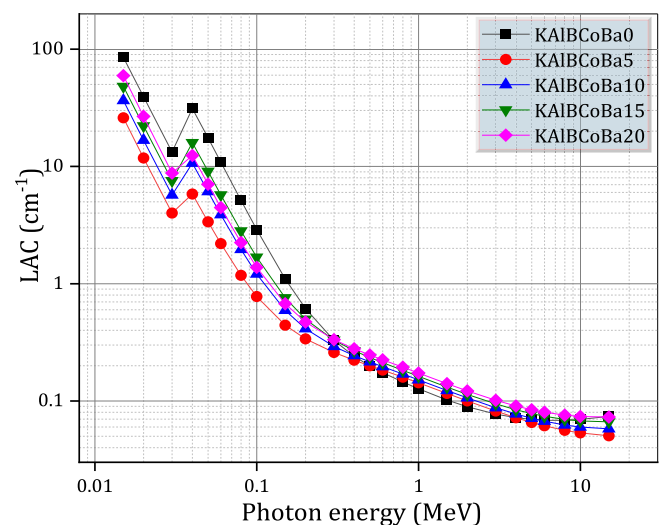


Fig. 14. The linear attenuation coefficient (LAC) as a function of the energy for KAlCoBa-glasses.

Poisson’s ratio lie in the range of 0.2 till 0.3. This range is the normal range of oxide glasses [36]. Such result of Poisson’s ratio indicates a relatively high cross-linked density. Further, the augmentation in values of Poisson’s ratio exhibits an increase in the number of structural bonds and consequently increases the system rigidity.

In this context, the obtained values of microhardness, Debye temperature and softening temperature were recorded in Figs. 5, 6a and 6b respectively and listed in Table 1, with their values of experimental error. Same reasons that explained the elastic moduli, it can also use to explain these additional informative parameters. Astonishingly, the increase in microhardness from 5.729 GPa reaching 5.948 GPa (increased to ~ 4%) is an indicator to the additions of barium oxide hardens the glassy network and increases the impact resistance and toughness of network. Furthermore, it is important to observe that the increase in softening temperature from 1082 K up to 1096 K with the increasing of barium contents in the borate glass matrix means more stability of the elastic characteristics of the glass structure, confirming that the alkalinity modifications have impacted role on the mechanical properties of the prepared glasses.

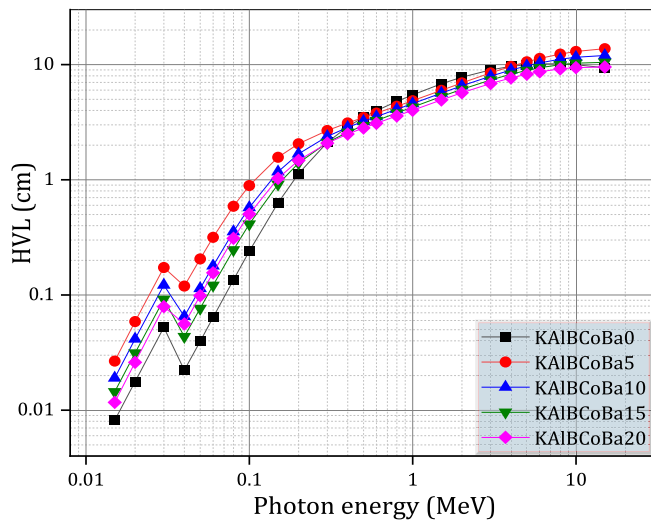


Fig. 15. The half value layer (HVL) as a function of the energy for KAIB-CoBa-glasses.

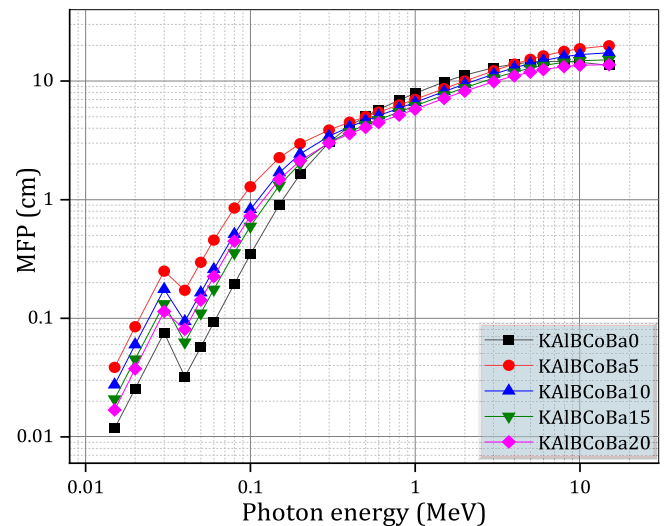


Fig. 17. The mean free path (MFP) as a function of the energy for KAIB-CoBa-glasses.

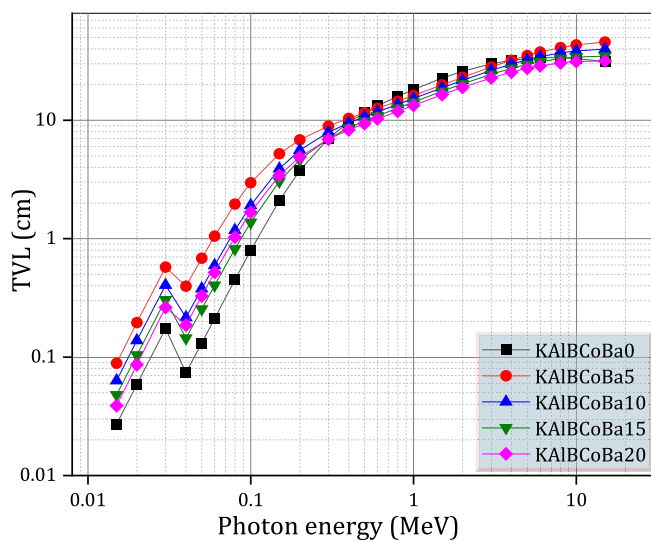


Fig. 16. The tenth value layer (TVL) as a function of the density for KAIB-CoBa-glasses.

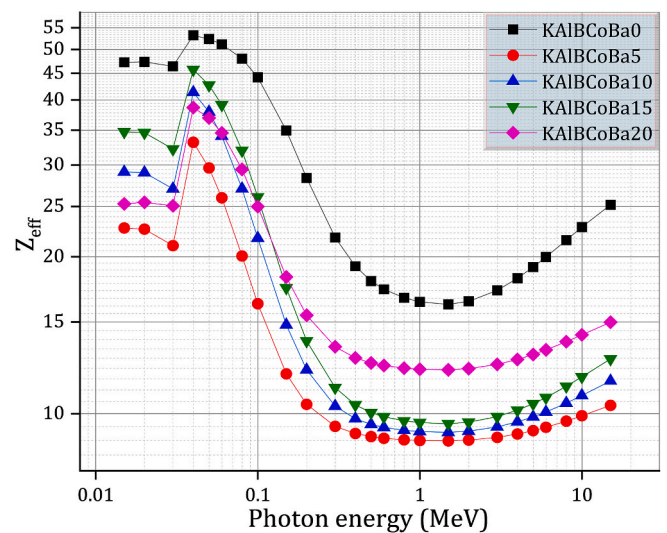


Fig. 18. The effective atomic number ( $Z_{eff}$ ) as a function of the energy for KAIBCoBa-glasses.

## 4.2. Optical properties

### 4.2.1. Optical band gap and Urbach energy

The typical optical absorption spectra of the prepared samples are displayed in Fig. 7. The optical absorbance spectra were recorded in ultraviolet (UV) and visible of electromagnetic spectrum. Normalization process was implemented on all spectra of samples.

Fundamentally, the absorption edges of the glassy specimens were observed to be a “single” absorption edge, assuring the high homogeneity of the prepared specimens and there is no existence of the phase separation. Such original absorption edges were found to undergo a clear blue shift with the progressive addition of alkaline content, predicting a widen in the optical band gaps. Important optical parameters are extracted from these edges such as the optical absorption coefficient ( $\alpha$ ) is computed from the well-known relationship:

$$\alpha = 2.303 * \text{Absorbance}/t \quad (15)$$

where  $t$  is the sample’s thickness. The obtained optical absorption spectra of glass specimens are displayed in Fig. 7. The  $\alpha$  was exploited to

calculate the optical band gaps ( $E_{opt}$ ) utilizing Davis and Mott relation [37,39,40]:

$$\alpha h\nu = m (h\nu - E_{opt})^n \quad (16)$$

herein, the index  $n$  takes the value of 2 corresponding to the indirect allowed electronic transitions model. Then, the optical band gaps are obtained from drawing the relation between  $h\nu$  as X-axis versus  $(\alpha h\nu)^{0.5}$  as Y-axis (i.e., Tauc’s plot). By extrapolating the first linear portions to  $(\alpha h\nu)^{0.5} = 0$ , then the intersection with X-axis directly gives the value of  $E_{opt}$ , as exhibited in Fig. 8. The outcome values of  $E_{opt}$  were displayed in Fig. 9. The  $E_{opt}$  of barium-free sample was 3.07 eV, then with the progressive additions of barium oxide contents, it jumped to be 3.58 eV for the highest barium content here involved. This obvious increase in the  $E_{opt}$  is related to alkalinity modulations representing in the bond length and bond strength. The increase in the  $E_{opt}$  originates from two factors: (i) the decrease in bond length, where the length of K–O is higher than that of Ba–O [38]. (ii) the increase in bond strength, where the strength of Ba–O (84 kJ/mol) is larger than that of K–O (50 kJ/mol) [41].

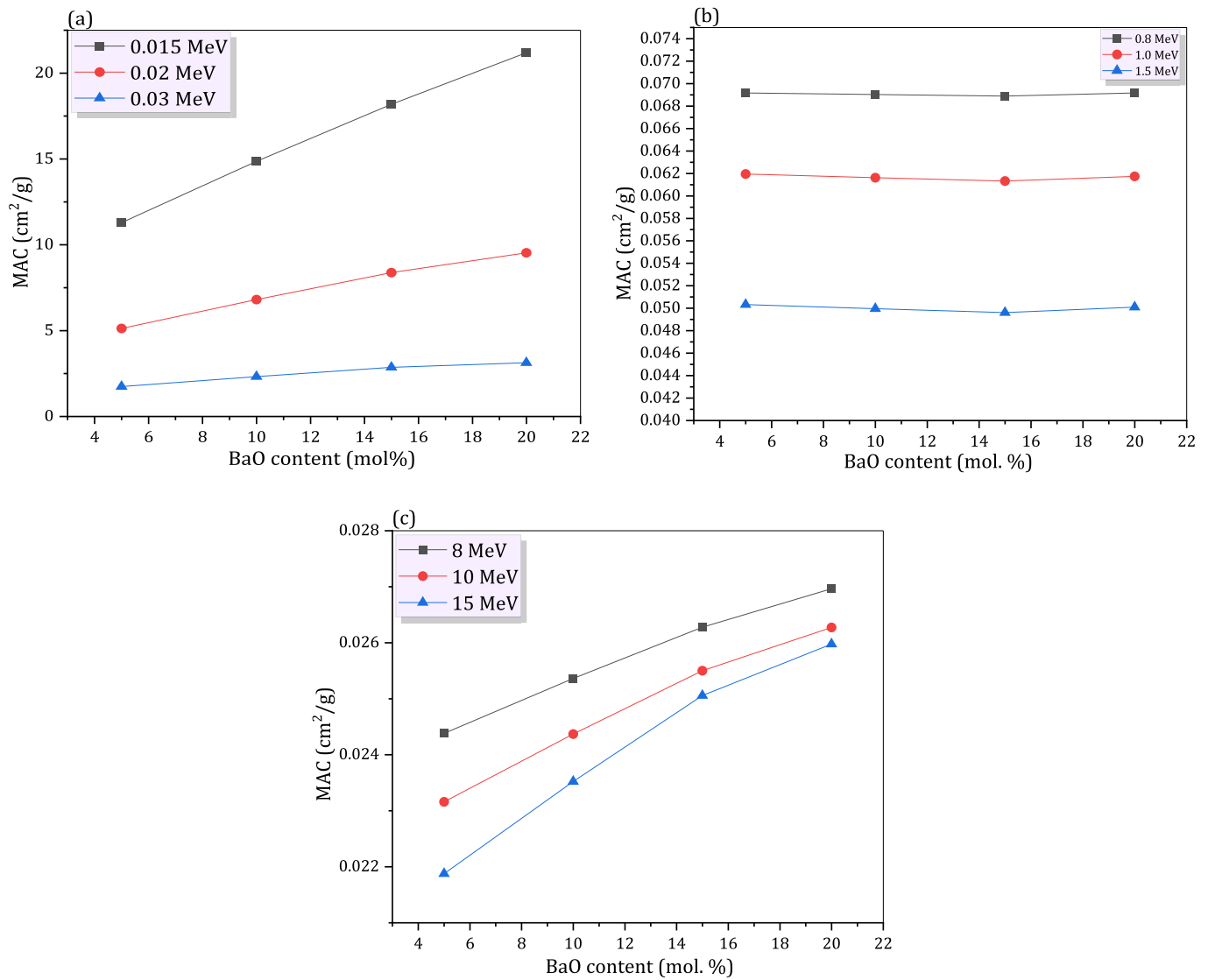


**Fig. 19.** (a, b and c): The mass attenuation coefficient versus BaO content for KAlBCoBa-glasses at (a) low energy range, (b) medium energy range and (c) high energy range.

Urbach tails correlates to the tail of electronic states density that extends between the valence and conduction bands [42–44]. In more detail, for oxide glass materials, the defect states are formed by the vacancies of oxygen in the glass matrix, making a disturbance in the band structure of sample. To understand the mechanism of Urbach tails occurrence, when the electromagnetic waves (light) are falling on the electrons in the excited states, these defects states catch them and prevent them from transferring to the conduction band, minimizing exponentially the absorbance process, causing the absorption tails in the optical absorption spectra. The energy-related these tails is known as Urbach energy, and it is determined by exponential relation between the absorption coefficients and the incident photons energy. The exponential relation used to calculate Urbach energy was proposed by F. Urbach [42–44] and given through:

$$\alpha = \text{constant} \exp[\hbar\nu(E_U)^{-1}] \quad (17)$$

by simplification of Eq. (17), by taking the logarithm of both sides of Eq. (17), one can get:

$$\text{Ln}(\alpha) = \text{Ln}(\eta) + \hbar\nu(E_U)^{-1} \quad (18)$$

Here,  $E_U$  values were found to mitigate with barium addition in glass

host. The alkalinity modifications by intercalation of barium oxide instead of potassium oxide into the network has a harsh impact on Urbach energy. The deterioration in Urbach energy is mainly related to the decrease in the disorder of samples with the addition of barium content. The substitution of  $\text{K}_2\text{O}$  by  $\text{BaO}$  makes the band tails less extended inside the band gaps energy. The introduction of  $\text{Ba}^{2+}$  ions (with high field strength) compared to  $\text{K}^+$  (with low field strength) ions leads to strength the bonding in the network, which minimizing the defects in the band gap. The healing of such band tails or defects pushes the absorption edges to shift toward the high energy (i.e., blue shift), this is a good agreement with behavior of  $E_{\text{opt}}$ .

#### 4.2.2. Optical constants

Metallization criterion ( $M$ ) is an effective parameter was established to forecast the metallicity behavior of samples. Metallization criterion could be computed based on optical band gaps values using the following relation [39–41]:

$$M = (E_{\text{opt}}/20)^{0.5} \quad (19)$$

The values of  $M$  ranges between two sets (0) and (1). The center between them is related to the semiconductor materials [43,45]. If  $M$

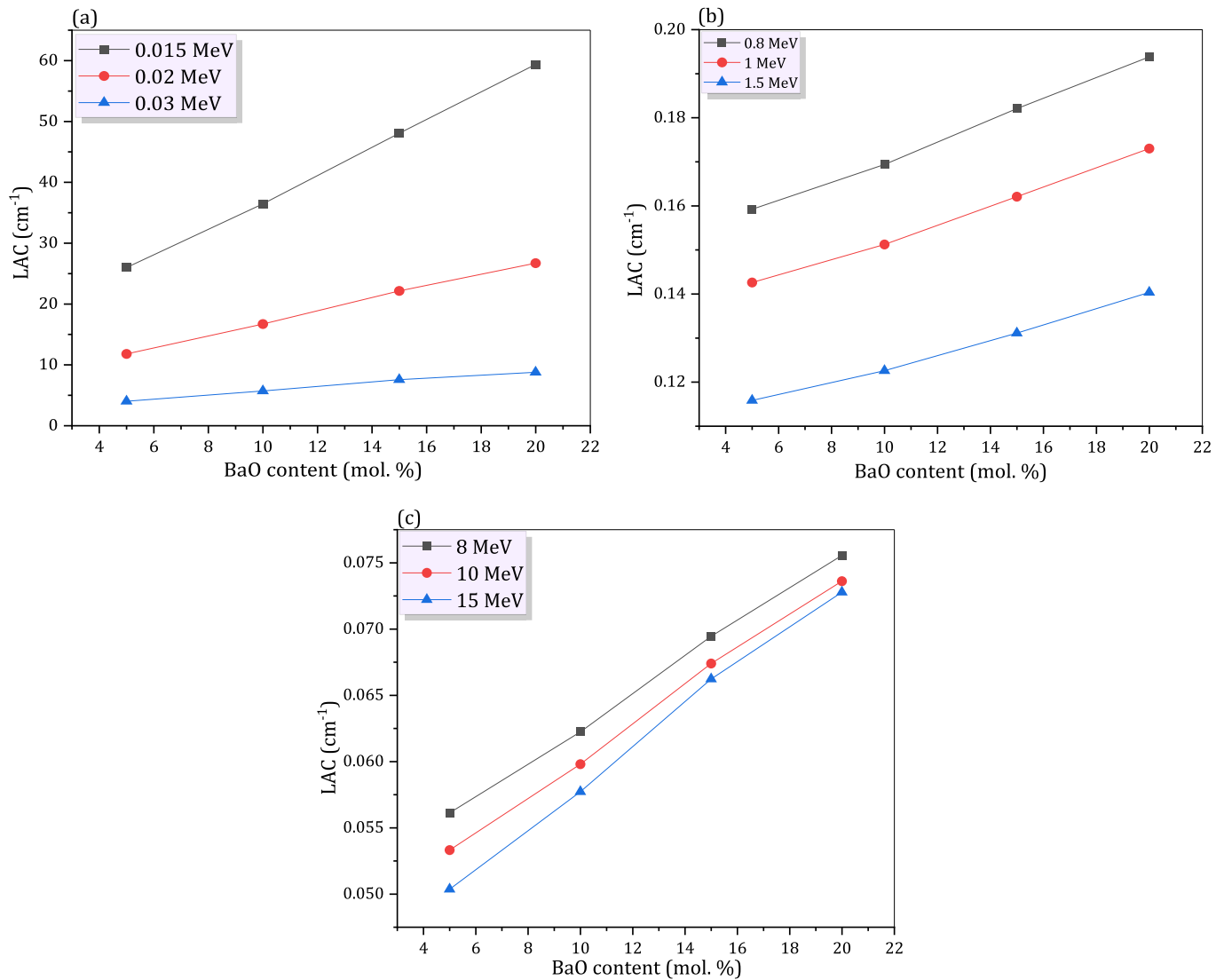


Fig. 20. (a–c): The linear attenuation coefficient versus BaO content for KAlCoBa-glasses at (a) low energy range, (b) medium energy range and (c) high energy range.

values near to (0), hence, the materials behave as metals. While the materials behave as dielectrics when  $M$  values near to (1). Here, the obtained values of  $M$  were furnished in Table 2. The increment in  $M$  values indicates that the glass samples tend to the dielectric nature with the progressive additions of barium contents.

Urbach energy is resulting from trapping the free electrons by the defect states. So, there is need to additional energy for controlling the interaction between these electrons. Therefore, the electron-phonon interaction parameters ( $E_{e-p}$ ) is known as “the interplay energy that is needed to bind two free electrons as pair states [40,46,47].  $E_U$  strongly contributes to calculating such electron-phonon interaction parameters from the mentioned relation in Ref. [33]. The obtained values of  $E_{e-p}$  were displayed in Table 2. One can notice the mitigation of this parameter, referring to the paucity of the free electrons in the glass matrix, therefore, there is no need for more phonon energies to pair the free electrons through the glassy matrix.

In addition, the velocity of light in space ( $c$ ) is divided by the velocity of light in the medium ( $v$ ) to determine the refractive index ( $n_0$ ). Estimated with Saad’s formula,  $n_0$  represents the path and propagation of electromagnetic radiations within materials and is thus the most important quantity [48],

$$n_0^2 = \sqrt{\frac{136.89 \text{ eV}}{E_{Opt}}} - 1 \quad (20)$$

The obtained values of refractive index of our KAlCoBa-glass samples are 2.38, 2.35, 2.31, 2.29 and 2.28 for KAlCoBBa0, KAlCoBBa5, KAlCoBBa10, KAlCoBBa15 and KAlCoBBa20 samples, respectively (as shown in Fig. 10). From this figure, we can detect the increased BaO doping produces a decrease in the  $n_0$  values. This behavior can be ascribed to the structural modifications and the increased values of  $E_{Opt}$  of KAlCoBa-glasses. Furthermore, the obtained increase is realized from the composition change. The addition of the high-density alkaline cations ( $Ba^{2+}$ ) at the cost of the low-density alkali cations ( $K^+$ ) leads to densification the network. This results in glassy specimens with a denser structures that minimizes the speed of light and rises the index of refraction [48,49]. Furthermore, the nonlinear optical susceptibility ( $\chi^{(3)}$ ) or nonlinear refractive index ( $n_2$ ) by using certain linear optical characteristics of glassy material. Therefore, the  $n_2$  and  $\chi^{(3)}$  are calculated from the  $E_g$  values through the Ticha-Tichy equation [50].

$$n_2 = \frac{B}{E_g^4}, B = 1.26 \times 10^{-9} [esu \text{ eV}^4] \quad (21)$$

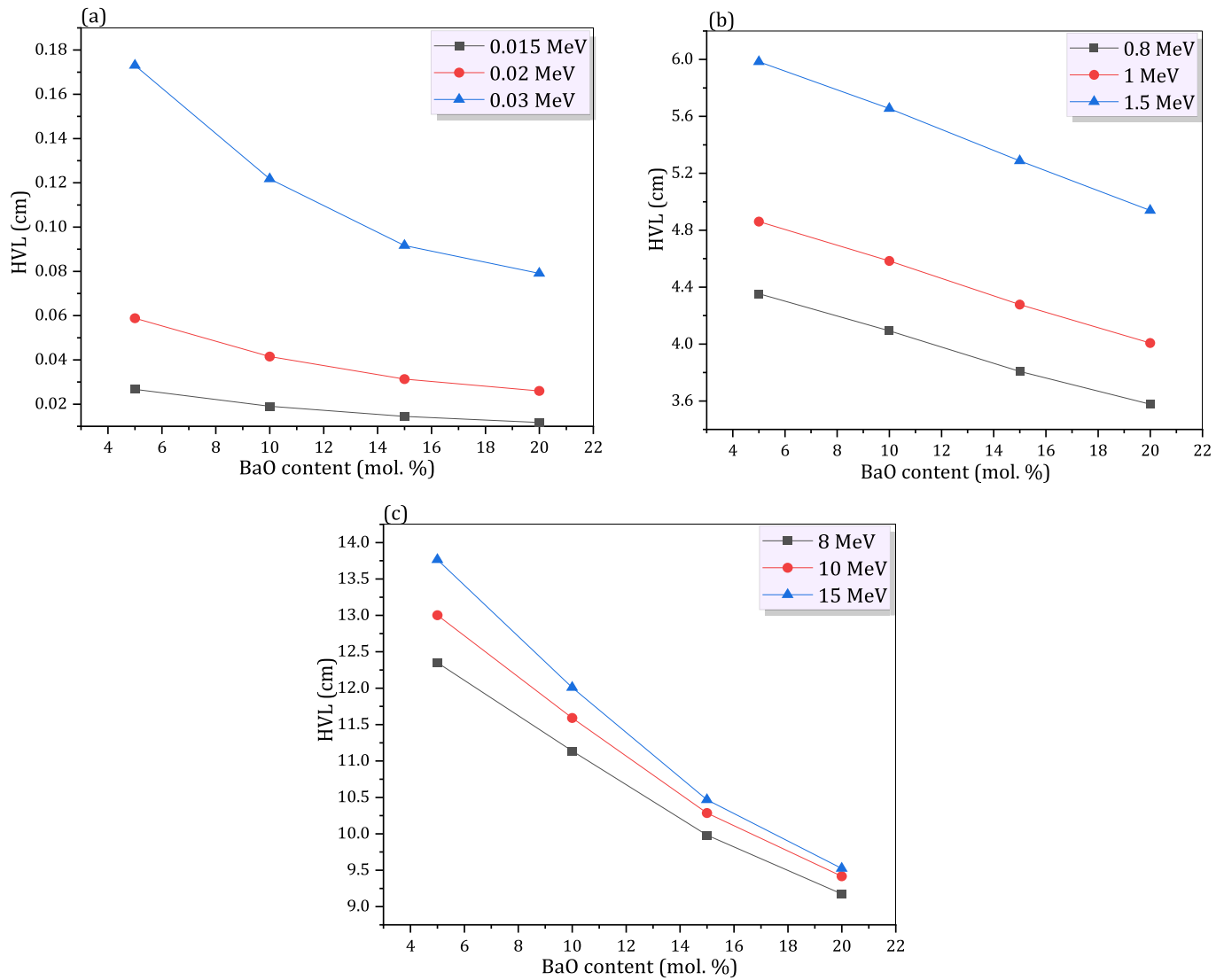


**Fig. 21.** (a–c): The half value layer versus BaO content for KAlCoBa-glasses at (a) low energy range, (b) medium energy range and (c) high energy range.

$$\chi^{(3)} = \left[ \frac{B}{(4\pi)^4} (n_o^2 - 1)^4 \right]; \quad B = 1.7 \times 10^{-10} \text{ (for } \chi^{(3)} \text{ in esu)} \quad (22)$$

The  $n_2$  values for all KAlCoBa-glasses are  $51.6 \times 10^{-10}$ ,  $45.2 \times 10^{-10}$ ,  $39.6 \times 10^{-10}$ ,  $36.4 \times 10^{-10}$  and  $34.5 \times 10^{-10}$  for KAlCoBa0, KAlCoBa5, KAlCoBa10, KAlCoBa15 and KAlCoBa20 glassy specimens, respectively (as shown in Fig. 11). The  $\chi^{(3)}$  values for all KAlCoBa-glasses are  $3.26 \times 10^{-12}$ ,  $2.82 \times 10^{-12}$ ,  $2.42 \times 10^{-12}$ ,  $2.21 \times 10^{-12}$  and  $2.09 \times 10^{-12}$  for KAlCoBa0, KAlCoBa5, KAlCoBa10, KAlCoBa15 and KAlCoBa20 glassy specimens, respectively (as shown in Fig. 12). The values of  $\chi^{(3)}$  and  $n_2$  demonstrate decreasing trends when BaO is added more. These trends are attributed to the decreased disorders [33], and the increased value of the optical band gaps for the glassy matrix [33].

### 4.3. Radiation shielding studies

#### 4.3.1. Energy dependence

The significance of pre-experimental considerations by means of mathematical and theoretical computations for radiation-shielding material is still a focus of intense research [7]. Herein, the Phy-X on-line software [34] was employed to calculate various radiation shielding characteristics of KAlCoBa-glasses, for example, the mass (MACs) and

linear (LACs) attenuation coefficient, half value layer (HVLs), tenth value layers (TVLs), mean free paths (MFP), and effective atomic number ( $Z_{\text{eff}}$ ) within the photons energies range 0.015–15 MeV. For KAlCoBa-glass, the MAC and LAC were computed and shown as against the photons energy (MeV) in Figs. 13 and 14 for various BaO additions (from 0 to 20 mol%). From Figs. 13 and 14, we can detect that the MACs and LACs values are greatest at lower photons energy; however, when the energy of photons is augmented from 0.015 to 0.03 MeV, the MACs and LACs values for all KAlCoBa-glasses show a quick reduction. Despite this quick decrease, a minor rise from 0.03 to 0.04 MeV is seen for all KAlCoBa-glasses. These behaviors can be described in terms of mechanisms of interaction of photons as follows: the photoelectric effects (PE) that describe how the photons interact with matter, this type of mechanisms favored at lower energy, and the interaction cross sections of (PE) proportionate to  $Z^{(4-5)}/E^{3.5}$  (where Z is the atomic numbers of the material and E is the photon energies). The rise from 0.03 to 0.04 MeV is caused by the K-shells absorption edges of high Z-numbers element, such as Ba, present in KAlCoBa-glasses. When the photons energy rises from 0.3 to 4 MeV (middle energy range), the MAC and LAC values for all KAlCoBa-glasses show a slow reduction. The change from fast reduction (at low energies) to slow reduction (at medium energies) can be related to that, the Compton scattering (CS) effect is predominated when photons energy rises from 0.3 to 4 MeV. Where, the

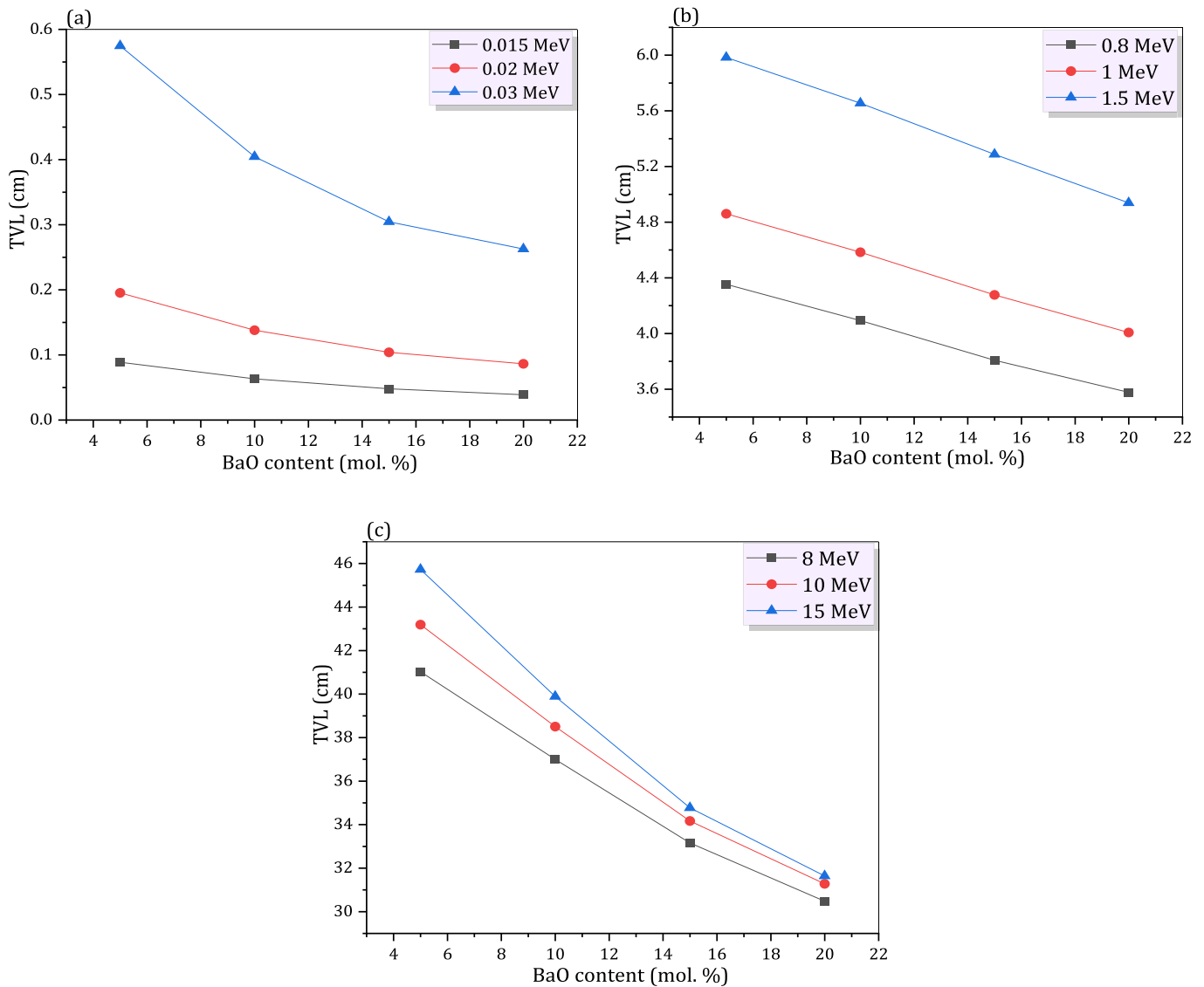


Fig. 22. (a–c): The tenth value layer versus BaO content for KAIBCoBa-glasses at (a) low energy range, (b) medium energy range and (c) high energy range.

Compton scattering cross-sections ( $\sigma_{CS}$ ) is inverse proportional to (E) and direct proportional to (Z) from the equation ( $\sigma_{CS} \propto Z/E$ ) [10]. More than 5 MeV (at high energies), the MAC and LAC values for all KAIBCoBa-glasses show the slowest reduction compared to other energy ranges. This behavior may be attributed to the dominating pair productions (PP) mechanism  $\sigma_{PP}$  is exactly proportional to ( $Z^2$ ) [7,51,52].

Additionally, the half value layer is crucial factor to determine the effectiveness of shielding materials (HVL). HVL is the thickness at which the intensity of photons is halved [51]. Similar to HVL, the tenth value layers (TVLs) refer to the thickness that reduces the intensity of photons to 1/10 of its initial values. Figs. 15 and 16 display the changes in HVL and TVL against the photon's energy for various BaO concentrations. HVL and TVL readings begin with minimal values from 0.015 to 0.03 MeV, then a sharp decrease is detected from 0.03 to 0.04 MeV. Then their values rapidly increase from 0.04 MeV to 15 MeV. All KAIBCoBa-glasses exhibit the same behaviors of HVL and TVL values against the photon energy. This phenomenon may be described as follows: at low energies, photoelectric processes need thin glasses (low values of HVLs and TVLs), but secondary Compton scattering necessitates thick glasses (large values of HVLs and TVLs) at medium energies [51]. In addition, when the photons have high energy levels, a substantial number of photons may penetrate the substance. Hence, a

thicker absorber is required to lower the quantity of transmitted photons by half or by a factor of ten [7,52].

Additionally, the mean free paths (MFPs) are a valuable measure for establishing the radiation-shielding capabilities of shielding materials. The relationship between MFP and LAC is  $MFP = 1/LAC$  [7,45]. Fig. 17 illustrates the dependence of MFP on photons energy for all KAIBCoBa-glass samples. The minimal MFP values begin between 0.015 and 0.03 MeV, then a sharp decrease is observed from 0.03 to 0.04 MeV. Then their values rapidly increase from 0.04 MeV to 15 MeV. According to these observations, the highest MFP corresponds to a photon energy of 15 MeV. The material can prevent a lower flux of photons with the greater energy and a higher flux of photons with the lower energy. Increases in MFP imply that thicker KAIBCoBa-glasses are preferable for radiation shielding applications.

$Z_{eff}$  is an additional crucial parameter that must be addressed in the radiations shielding fields. This quantity quantifies the effectiveness of a radiations shielding materials. Where the shielding capacity of more material relates to bigger  $Z_{eff}$  values. This indicates that more photons are absorbed by materials with high  $Z_{eff}$  values [52]. Fig. 18 depicts the relationship between  $Z_{eff}$  and photon energies for all KAIBCoBa-glasses. Fig. 18 demonstrates that  $Z_{eff}$  values decrease as photons energies increase from 0.015 to 0.03 MeV, and subsequently rise significantly as

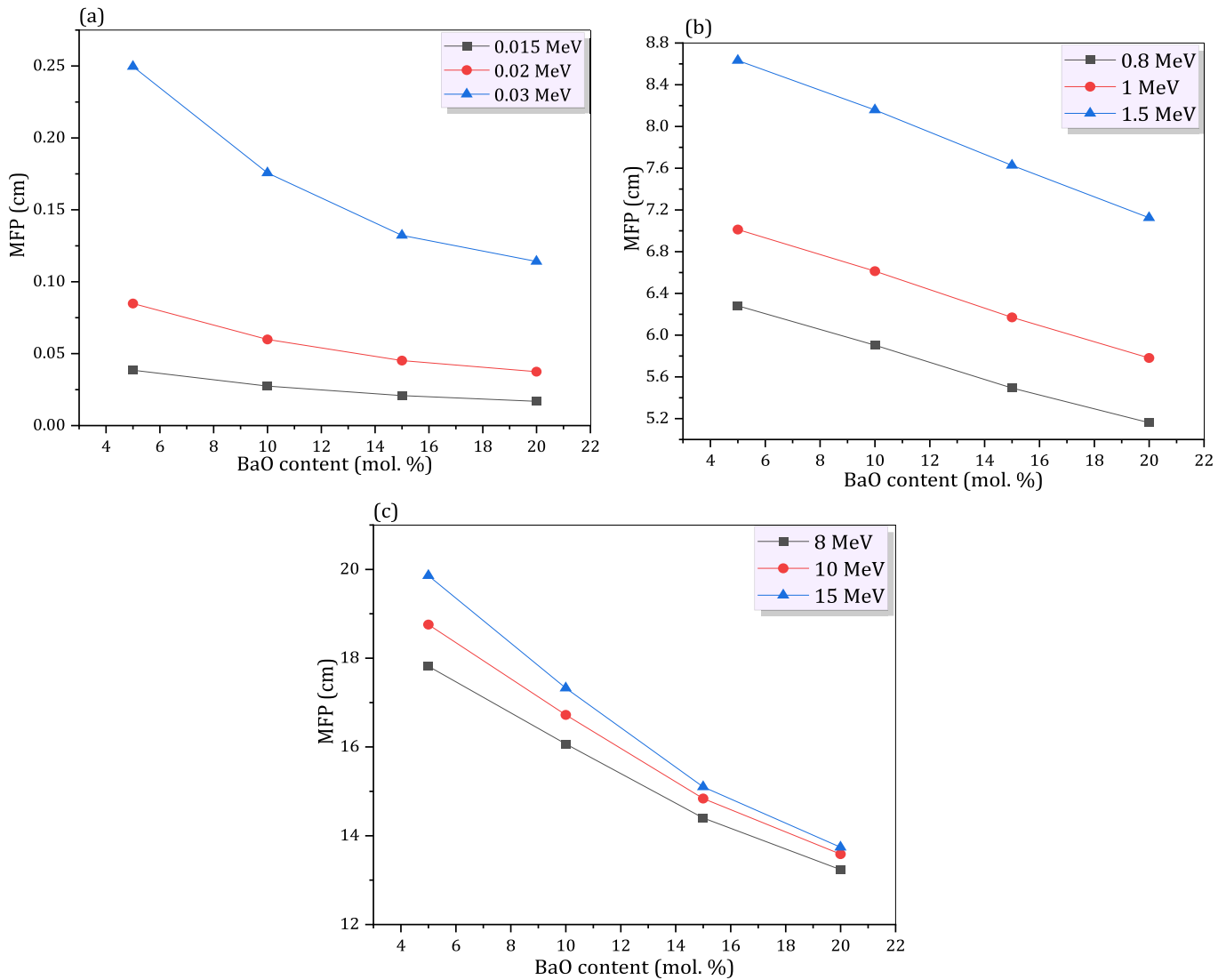


Fig. 23. (a–c): The mean free path versus BaO content for KAIBCoBa-glasses at (a) low energy range, (b) medium energy range and (c) high energy range.

photon energies increase from 0.03 to 0.04 MeV which may be ascribed to photoelectric absorption, where the interaction cross sections of (PE) proportionate to  $Z^{(4-5)}/E^{3.5}$  [52,53]. Then the values diminish significantly as energy of photon raises from 0.04 to 1 MeV. This can be ascribed to the predominance of CS in this energies range and the fact that  $\sigma_{CS}$  has inverse proportionate to (E) and has a direct proportionality to (Z) agreeing to the equation ( $\sigma_{CS} \propto Z/E$ ). In addition, an obvious rise is seen from 1 to 15 MeV. Because of the prevalence of the PP interactions in which the pairs formation cross section ( $\sigma_{pp}$ ) is has a direct proportional to ( $Z^2$ ), this rise in  $Z_{eff}$  values is seen for higher energy photons [54].

#### 4.3.2. Compositions dependence

Fig. 19(a–c) and 20 (a–c) depict the variations of MACs and LACs vs BaO concentration as typical figures for sequence of energies (lower, medium and higher energy) from 0.015 to 15 MeV. We see a clear influence of BaO additions on the values of MACs and LACs. Both parameters exhibit increasing trends for low, middle, and high energies with further BaO additions from 5 to 20 mol%. These behaviours may be explained by the influence of BaO on the structural variations within KAIBCoBa-glasses, such as their increasing density from 2.120 g/cm<sup>3</sup> to 2.802 g/cm<sup>3</sup>. It is generally recognised that density is one of the most important criteria for enhancing a medium's capacity to attenuate

photons of radiation. In addition, the two parameters (MACs and LACs) are dependent not only on photon energy but also on the shield's density. The photons energies affect the changes produced in MACs and LACs with the density.

As presented in Fig. 21(a–c) and Fig. 22(a–c), the values of HVLs and TVLs decreased as the BaO concentration rose from 5 to 20 mol% in the lower, medium, and higher energies from 0.015 to 15 MeV. This is because of the inverse relationships between density and HVLs and TVLs; when BaO concentration increases, the density of KAIBCoBa-glasses increases, resulting in decreasing behaviours for HVLs and TVLs. Lower HVL and TVL values suggest better and enhanced radiation shielding characteristics. In this instance, the inclusion of BaO instead of K<sub>2</sub>O reduces both HVL and TVL, reflecting the positive effects of BaO on the shielding characteristics of KAIBCoBa-glasses. In addition, Fig. 21 (a–c) and Fig. 22(a–c) reveal that the slope of HVLs and TVLs vs BaO curves at high energies are greater than those at low energies. At high energy levels, BaO has noticeable influences (decreasing behaviours) on both the HVLs and TVLs of KAIBCoBa-glasses.

Instead, Fig. 23 (a, b, and c) demonstrates that the increases of BaO resulted in decreased MFP values for the lower, medium, and higher energies range from 0.015 to 15 MeV. These decreases are a result of the augmentation in density, that is accountable for the reduction in MFP values. In addition, Fig. 23(a–c) reveals that the slope of the MFP vs BaO

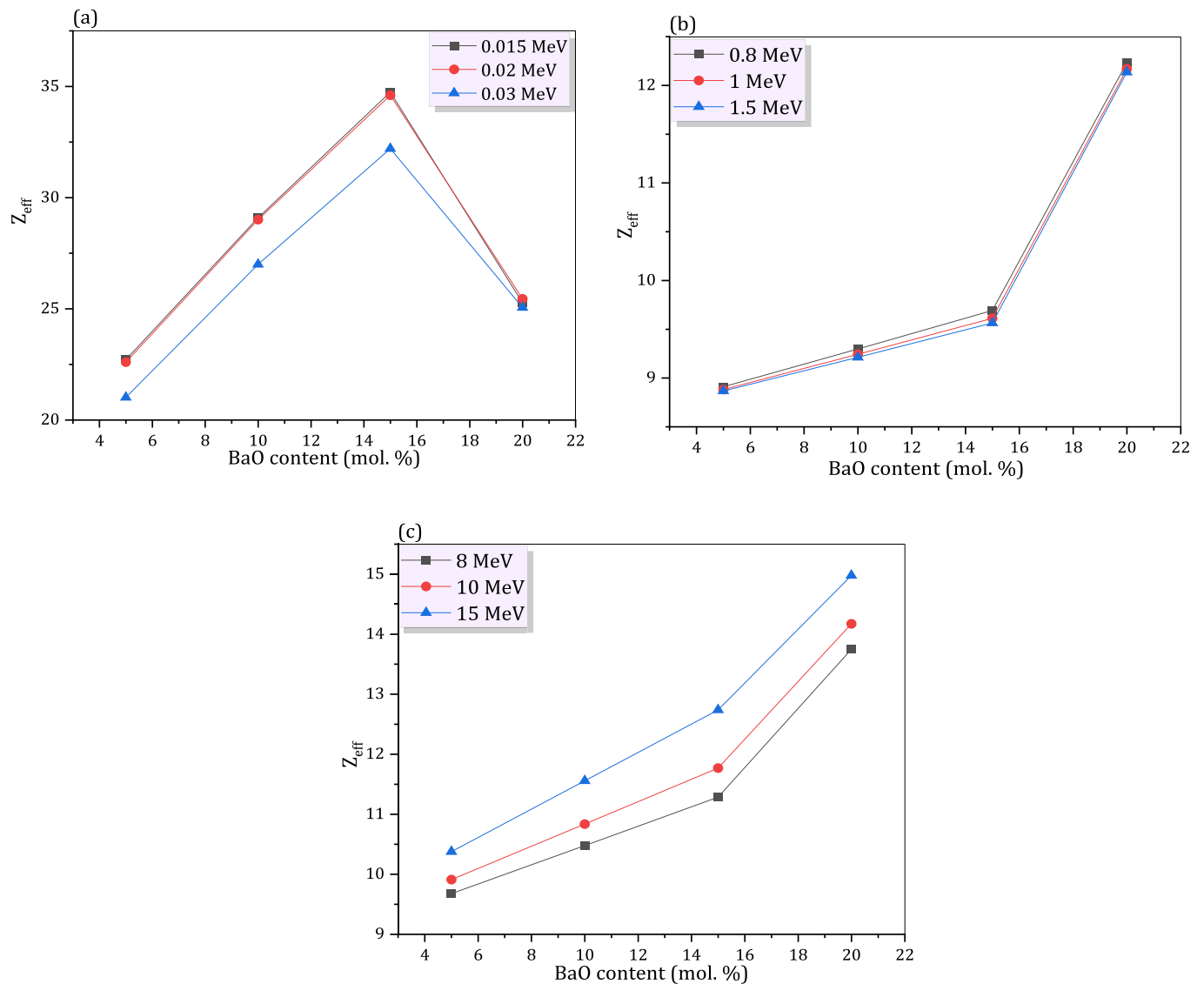


Fig. 24. (a–c): The effective atomic number versus BaO content for KAIBCoBa-glasses at (a) low energy range, (b) medium energy range and (c) high energy range.

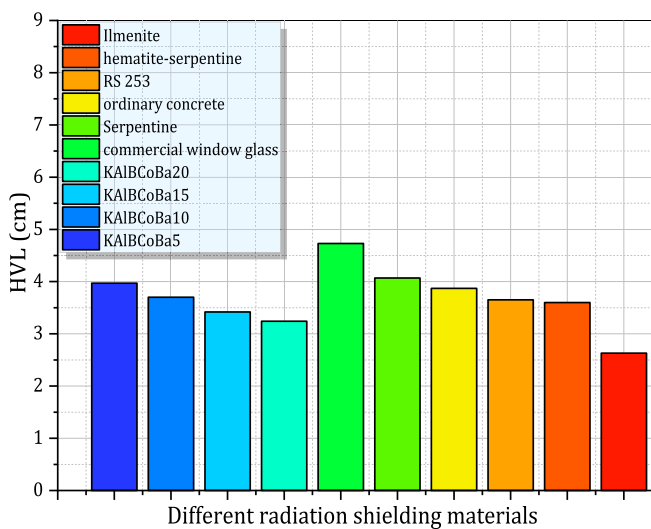


Fig. 25. The half value layer (HVL) of the KAIBCoBa-glasses in comparison to some standard shielding materials at 0.662 MeV.

curves at higher energy are steeper than those at lower energy. At high energy levels, BaO has a noticeable influence on KAIBCoBa-glasses. The significance of density is that: it determines the thickness required to attenuate certain target radiations level is further emphasised by these findings. The different shields attenuate the smallest quantities of radiations at the greatest energy values. This suggests that the increments in photons energy is proportional to the increase in MFPs values and therefore thicker KAIBCoBa-glasses are needed for certain applications.

Fig. 24(a–c) demonstrated that increases of BaO resulted in increased  $Z_{eff}$  value for the lower, medium, and higher energies range of 0.015–15 MeV. Results for  $Z_{eff}$  values exhibit comparable tendencies to MAC and LAC values. For KAIBCoBa-glasses at various energy ranges,  $Z_{eff}$  values are directly related to BaO concentration. In other words,  $Z_{eff}$  values exhibit the trends KAIBCoBa20 > KAIBCoBa15 > KAIBCoBa10 > KAIBCoBa5 throughout all energy ranges. This response of  $Z_{eff}$  demonstrates once again that the greater the BaO concentration in glasses materials, the better their radiation-shielding properties. regarding to the  $Z_{eff}$  values, the KAIBCoBa20 glassy specimen has the best shielding characteristics compared to KAIBCoBa-glasses.

#### 4.3.3. Comparing KAlBCoBa-glasses to well-known shielding glasses and concretes

In order to use KAlBCoBa-glasses as radiation shields, it is necessary to compare all KAlBCoBa-glasses with other well-known shielding glasses and concretes, such as commercial windows glasses, popular, Ilmenite, Hematite serpentine and serpentine concretes and SCHOOT RS253. This comparison is shown in Fig. 25, which comprise the values of the HVLs for at 0.662 MeV. The HVLs values were investigated in Refs. [55–58]. Examining Fig. 25, we see that the HVL values of all KAlBCoBa20 glass specimen is less than those of the shielding glasses and concretes except Ilmenite concretes. Thus, we can assert that our glassy specimens employed in radiation shielding applications have exceptional shielding capability.

## 5. Conclusion

The addition of barium oxide enhanced the elastic moduli, confirming a high cross-linked density, high impact resistance and toughness of the network, with a good mechanical stability of samples. In detail, from the free-barium specimen to the maximum content of barium oxide here involved, it is observed that the shear modulus increased from 33.8 GPa reaching 37.7 GPa (increased to ~ 11.5%), while longitudinal modulus enhanced from 100.5 GPa up to 117.4 GPa (enhanced to ~ 16.8%), besides Young's modulus augmented from 84.4 GPa to 95.3 GPa (augmented to ~ 13%), the last modulus is bulk that increased from 55.4 GPa reaching 67.2 GPa (increased to ~ 21.3%). This increase in the elastic moduli resulted from introduced barium oxide instead of potassium oxide from 0 mol % to 20 mol %. Furthermore, the effectiveness of radiations shielding of the KAlBCoBa glass samples were studied and compared to those of well-known radiation protection materials. The comparison confirmed that the glassy sample with the maximum barium oxide content is better than the well-known radiation shielding materials and is suitable for use in radiation shielding application, especially at low energies.

## CRedit authorship contribution statement

**A. Samir:** Sample preparation, measurements, Writing – review & editing. **Moukhtar A. Hassan:** Conceptualization, Sample preparation, Formal analysis, Writing – review & editing. **F. Ahmad:** Formal analysis, Writing – review & editing. **M.S. Sadeq:** Formal analysis, Writing – review & editing. **S.Y. Marzouk:** Formal analysis, Writing – review & editing. **H.Y. Morshidy:** Sample preparation, measurements, Formal analysis, Writing – review & editing.

## Declaration of competing interest

The authors declare that they have no known competing financial interests or personal relationships that could have appeared to influence the work reported in this paper.

## Data availability

Data will be made available on request.

## References

- R. Kurtulus, M.I. Sayyed, T. Kavas, K.A. Mahmoud, O.L. Tashlykov, M. U. Khandaker, D.A. Bradley, A lanthanum-barium-borovanadate glass containing Bi<sub>2</sub>O<sub>3</sub> for radiation shielding applications, *Radiat. Phys. Chem.* 186 (2021), 109557, <https://doi.org/10.1016/j.radphyschem.2021.109557>.
- M.I. Sayyed, T.A. Elmosalami, M.A. Abdo, M.S. Sadeq, Optical and radiation shielding features of NiO-CdO-BaO borosilicate glasses, *Phys. Scripta* 97 (2022), <https://doi.org/10.1088/1402-4896/ac7984>.
- M.A.M. Uosif, A.M.A. Mostafa, S.A.M. Issa, H.O. Tekin, Z.A. Alrowaili, O. Kilicoglu, Structural, mechanical and radiation shielding properties of newly developed tungsten lithium borate glasses: an experimental study, *J. Non-Cryst. Solids* 532 (2020), 119882, <https://doi.org/10.1016/j.jnoncrysol.2019.119882>.
- A. Tasnim, M.H. Sahadath, M.N. Islam Khan, Development of high-density radiation shielding materials containing BaSO<sub>4</sub> and investigation of the gamma-ray attenuation properties, *Radiat. Phys. Chem.* 189 (2021), 109772, <https://doi.org/10.1016/j.radphyschem.2021.109772>.
- M.S. Sadeq, I.I. Bashter, S.M. Salem, S.F. Mansour, H.A. Saudi, M.I. Sayyed, G. Mostafa, Progress in Nuclear Energy Enhancing the gamma-ray attenuation parameters of mixed bismuth/barium borosilicate glasses : using an experimental method , Geant4 code and XCOM software, *Prog. Nucl. Energy* 145 (2022), 104124, <https://doi.org/10.1016/j.pnucene.2022.104124>.
- M.K. Hamad, M.I. Sayyed, M.H.A. Mhareb, M.S. Sadeq, N. Dwaikat, M. A. Almessiere, K.A. Ziq, Effects of TiO<sub>2</sub>, V<sub>2</sub>O<sub>5</sub>, MnO<sub>2</sub> and Ti<sub>2</sub>O<sub>3</sub> on structural, physical, optical and ionizing radiation shielding properties of strontium borotellurite glass: an experimental study, *Opt. Mater.* 127 (2022), 112350, <https://doi.org/10.1016/j.optmat.2022.112350>.
- M. Ezzeldin, L.M. Al-harbi, M.S. Sadeq, A.E. Mahmoud, M.A. Muhammad, H. A. Ahmed, Impact of CdO on optical , structural , elastic , and radiation shielding parameters of CdO – PbO – ZnO – B<sub>2</sub>O<sub>3</sub> – SiO<sub>2</sub> glasses, *Ceram. Int.* (2023), <https://doi.org/10.1016/j.ceramint.2023.03.042>.
- E. Kavaz, H.O. Tekin, O. Agar, E.E. Altunsoy, O. Kilicoglu, M. Kamislioglu, M. M. Abuzaid, M.I. Sayyed, The mass stopping power/projected range and nuclear shielding behaviors of barium bismuth borate glasses and influence of cerium oxide, *Ceram. Int.* 45 (2019) 15348–15357.
- M.A.M. Uosif, A.M.A. Mostafa, Shams A.M. Issa, H.O. Tekin, Z.A. Alrowaili, O. Kilicoglu, Structural, mechanical and radiation shielding properties of newly developed tungsten lithium borate glasses: an experimental study, *J. Non-Cryst. Solids* 532 (2020), 119882.
- Salavadi Stalin, D.K. Gaikwad, M.S. Al-Buriah, Ch Srinivasu, Shaik Amer Ahmed, H.O. Tekin, Syed Rahman, Influence of Bi<sub>2</sub>O<sub>3</sub>/WO<sub>3</sub> substitution on the optical, mechanical, chemical durability and gamma ray shielding properties of lithium-borate glasses, *Ceram. Int.* 47 (2021) 5286–5299.
- A.M.A. Mostafa, Shams A.M. Issa, Hesham M.H. Zakaly, M.H.M. Zaid, H.O. Tekin, K.A. Matori, H.A.A. Sidek, R. Elsaman, The influence of heavy elements on the ionizing radiation shielding efficiency and elastic properties of some tellurite glasses: theoretical investigation, *Results Phys.* 19 (2020), 103496.
- M.H.A. Mhareb, Physical, optical and shielding features of Li<sub>2</sub>O-B<sub>2</sub>O<sub>3</sub>-MgO-Er<sub>2</sub>O<sub>3</sub> glasses co-doped of Sm<sub>2</sub>O<sub>3</sub>, *Appl. Phys. Mater. Sci. Process* 126 (2020) 1–8, <https://doi.org/10.1007/s00339-019-3262-9>.
- S. Kaewjaeng, J. Kaewkhao, P. Limsuwan, U. Maghanemi, Effect of BaO on optical, physical and radiation shielding properties of SiO<sub>2</sub>-B<sub>2</sub>O<sub>3</sub>-Al<sub>2</sub>O<sub>3</sub>-CaO- Na<sub>2</sub>O glasses system, *Procedia Eng.* 32 (2012) 1080–1086, <https://doi.org/10.1016/j.proeng.2012.02.058>.
- H.M.H. Zakaly, H.A. Saudi, S.A.M. Issa, M. Rashad, A.I. Elazaka, O. Tekin, Y. B. Saddeek, Alteration of optical , structural , mechanical durability and nuclear radiation attenuation properties of barium borosilicate glasses through BaO reinforcement : experimental and numerical analyses, *Ceram. Int.* 47 (2021) 5587–5596, <https://doi.org/10.1016/j.ceramint.2020.10.143>.
- N.K. Libeesh, K.A. Naseer, K.A. Mahmoud, M.I. Sayyed, S. Arivazhagan, M. S. Alqahtani, E.S. Yousef, M.U. Khandaker, Applicability of the multispectral remote sensing on determining the natural rock complexes distribution and their evaluability on the radiation protection applications, *Radiat. Phys. Chem.* 193 (2022), 110004, <https://doi.org/10.1016/j.radphyschem.2022.110004>.
- P.E. Teresa, R. Divina, K.A. Naseer, K. Marimuthu, Study on the luminescence behavior of Dy<sup>3+</sup> ions activated, modifier dependent alkali boro-tellurite glasses for white LED application, *Optik* 259 (2022), 169024, <https://doi.org/10.1016/j.ijleo.2022.169024>.
- M.A. Imheidat, M. KhHamad, K.A. Naseer, M.I. Sayyed, N. Dwaikat, K. Cornish, Y. S. Alajerami, M. Alqahtani, M.H.A. Mhareb, Radiation shielding, mechanical, optical, and structural properties for tellurite glass samples, *Optik* 268 (2022), 169774, <https://doi.org/10.1016/j.ijleo.2022.169774>.
- M.H.A. Mhareb, M. Alqahtani, F. Alshahri, Y.S.M. Alajerami, N. Saleh, N. Alonizan, M.I. Sayyed, M.G.B. Ashiq, T. Ghrib, S.I. Al-dhafar, T. Alayed, M.A. Morsy, The impact of barium oxide on physical , structural , optical , and shielding features of sodium zinc borate glass, *J. Non-Cryst. Solids* 541 (2020), 120090, <https://doi.org/10.1016/j.jnoncrysol.2020.120090>.
- D.A. Aloraini, A. Kumar, A.H. Almuqrin, M.I. Sayyed, Optical and gamma ray shielding properties BaO doped K<sub>2</sub>O-TiO<sub>2</sub>-P<sub>2</sub>O<sub>5</sub> glasses, *Optik* 247 (2021), 167893, <https://doi.org/10.1016/j.ijleo.2021.167893>.
- D.A. Aloraini, M.Y. Hanfi, M.I. Sayyed, K.A. Naseer, A.H. Almuqrin, P. Tamayo, O. L. Tashlykov, K.A. Mahmoud, Design and gamma-ray attenuation features of new concrete materials for low- and moderate-photons energy protection applications, *Materials* 15 (2022) 4947, <https://doi.org/10.3390/ma15144947>.
- M.U. Khandaker, D.A. Bradley, H. Osman, M.I. Sayyed, A. Sulieman, M.R. I. Faruque, K.A. Naseer, A.M. Idris, The significance of nuclear data in the production of radionuclides for theranostic/therapeutic applications, *Radiat. Phys. Chem.* 200 (2022), 110342, <https://doi.org/10.1016/j.radphyschem.2022.110342>.
- S. Arunkumar, K.A. Naseer, M. Yousof Ameen, K.A. Mahmoud, M.I. Sayyed, K. Marimuthu, D. James Silvia, R. Divina, M.S. Alqahtani, E.S. Yousef, Physical, structural, optical, and radiation screening studies on Dysprosium ions doped Niobium Bariumtelluroborate glasses, *Radiat. Phys. Chem.* 204 (2023), 110669, <https://doi.org/10.1016/j.radphyschem.2022.110669>.
- M.I. Sayyed, N. Dwaikat, M.H.A. Mhareb, A.N. D'Souza, N. Almousa, Y.S. M. Alajerami, F. Almasoud, K.A. Naseer, S.D. Kamath, M.U. Khandaker, H. Osman, S. Alamri, Effect of TeO<sub>2</sub> addition on the gamma radiation shielding competence and mechanical properties of boro-tellurite glass: an experimental approach,

- J. Mater. Res. Technol. 18 (2022) 1017–1027, <https://doi.org/10.1016/j.jmrt.2022.02.130>.
- [24] S.A. Bassam, K.A. Naseer, V.K. Keerthana, P. Evangelin Teresa, C.S. Suchand Sangeeth, K.A. Mahmoud, M.I. Sayyed, M.S. Alqahtani, E. El Shiekh, M. U. Khandaker, Physical, structural, elastic and optical investigations on Dy<sup>3+</sup> ions doped boro-tellurite glasses for radiation attenuation application, *Radiat. Phys. Chem.* 206 (2023), 110798, <https://doi.org/10.1016/j.radphyschem.2023.110798>.
- [25] S.A. Bassam, K.A. Naseer, A.J. Prakash, K.A. Mahmoud, C.S. SuchandSangeeth, M. I. Sayyed, M.S. Alqahtani, E. El Sheikh, M.U. Khandaker, Effect of Tm<sup>2O3</sup> addition on the physical, structural, elastic, and radiation-resisting attributes of tellurite-based glasses, *Radiat. Phys. Chem.* 209 (2023), 110988, <https://doi.org/10.1016/j.radphyschem.2023.110988>.
- [26] M. Yamane, J.D. Mackenzie, Vicker's hardness of glass, *J. Non-Cryst. Solids* 15 (1974) 153–164.
- [27] S. Inaba, S. Fujino, Mechanical properties of glass, *New Glass* 23 (2008) 46–52.
- [28] R.J. Hand, D.R. Tadjiev, Mechanical properties of silicate glasses as a function of composition, *J. Non-Cryst. Solids* 356 (2010) 2417–2423.
- [29] A. Makishima, J.D. Mackenzie, Direct calculation of Young's modulus of glass, *J. Non-Cryst. Solids* 12 (1973) 35–45.
- [30] A. Makishima, J.D. Mackenzie, Calculation of bulk modulus, shear modulus and Poisson's ratio of glass, *J. Non-Cryst. Solids* 17 (1975) 147–157.
- [31] S. Dériano, T. Rouxel, M. Lefloch, B. Beuneu, Structure and mechanical properties of alkali-alkaline earth-silicate glasses, *Phys. Chem. Glasses* 45 (2004) 37–44.
- [32] S. Bhattacharya, H.D. Shashikala, Effect of BaO on thermal and mechanical properties of alkaline earth borosilicate glasses with and without Al<sub>2</sub>O<sub>3</sub>, *Phys. B Condens. Matter* 571 (2019) 76–86, <https://doi.org/10.1016/j.physb.2019.06.065>.
- [33] E. Şakar, Ö.F. Özpolat, B. Alım, M.I. Sayyed, M. Kurudirek, Phy-X/PSD: development of a user friendly online software for calculation of parameters relevant to radiation shielding and dosimetry, *Radiat. Phys. Chem.* 166 (2020), 108496, <https://doi.org/10.1016/j.radphyschem.2019.108496>.
- [34] F. Ahmad, E. Nabhan, Spectroscopic and mechanical studies of lithium aluminoborate glasses doped with chromium ions, *Opt. Quant. Electron.* 51 (2019) 1–14, <https://doi.org/10.1007/s11082-019-1973-y>.
- [35] S.N. Nazrin, M.K. Halimah, F.D. Muhammad, A.A. Latif, S.M. Iskandar, S. Asyikin, Experimental and theoretical models of elastic properties of erbium-doped zinc tellurite glass system for potential fiber optic application, *Mater. Chem. Phys.* 259 (2021), 123992, <https://doi.org/10.1016/j.matchemphys.2020.123992>.
- [36] U. Veit, C. Rüssel, Density and Young's Modulus of ternary glasses close to the eutectic composition in the CaO – Al<sub>2</sub>O<sub>3</sub> – SiO<sub>2</sub> -system, *Ceram. Int.* 42 (2016) 5810–5822, <https://doi.org/10.1016/j.ceramint.2015.12.123>.
- [37] N.F. Mott, E.A. Davis, *Electronic Processes in Non-crystalline Materials*, second ed., Oxford University Press, Oxford, 1977.
- [38] M.G. Moustafa, H. Morshidy, A.R. Mohamed, M.M. El-Okr, A comprehensive identification of optical transitions of cobalt ions in lithium borosilicate glasses, *J. Non-Cryst. Solids* 517 (2019) 9–16, <https://doi.org/10.1016/j.jnoncrysol.2019.04.037>.
- [39] M.M. El-Hady, H.Y. Morshidy, M.A. Hassan, Judd-Ofelt analysis, optical and structural features of borate glass doped with erbium oxide, *J. Lumin.* 263 (2023), 119972, <https://doi.org/10.1016/j.jlumin.2023.119972>.
- [40] H.Y. Morshidy, A.R. Mohamed, A.A. Abul-magd, M.A. Hassan, Ascendancy of Cr<sup>3+</sup> on Cr<sup>6+</sup> valence state and its effect on borate glass environment through CdO doping, *Mater. Chem. Phys.* 285 (2022), 126128, <https://doi.org/10.1016/j.matchemphys.2022.126128>.
- [41] V. Dimitrov, T. Komatsu, An interpretation of optical properties of oxides and oxide glasses in terms of the electronic ion polarizability and average single bond strength, *J. Univ. Chem. Technol. Metall.* 45 (2010) 219–250, <https://doi.org/10.1016/j.jnoncrysol.2009.11.014>.
- [42] F. Urbach, The long-wavelength edge of photographic sensitivity and of the electronic Absorption of Solids [8], *Phys. Rev.* 92 (1953) 1324, <https://doi.org/10.1103/PhysRev.92.1324>.
- [43] S.A. Hussien, E.M. Saad, E.A. Gaber, A.E. razek Mahmoud, H.Y. Morshidy, Impactive cadmium modifications to enhance the structural-optical relationship in nickel borate glasses, *Ceram. Int.* (2023), <https://doi.org/10.1016/j.ceramint.2023.04.124>.
- [44] M. Ezzeldien, H.Y. Morshidy, A.M. Al-boajan, A.M. Al Souwaileh, Z.A. Alrowaili, M.S. Sadeq, Environmental impacts of La<sub>2</sub>O<sub>3</sub> on the optical and ligand field parameters of Ni ions inside Na<sub>2</sub>O-B<sub>2</sub>O<sub>3</sub> glass, *J. Alloys Compd.* 961 (2023), 170891, <https://doi.org/10.1016/j.jallcom.2023.170891>.
- [45] S.F. Mansour, S. Wageh, M.F. Alotaibi, M.A. Abdo, M.S. Sadeq, Impact of bismuth oxide on the structure, optical features and ligand field parameters of borosilicate glasses doped with nickel oxide, *Ceram. Int.* 47 (2021) 21443–21449.
- [46] H.Y. Morshidy, A.R. Mohamed, A.A. Abul-magd, M.A. Hassan, Role of high energy Cr<sup>6+</sup> optical transition induced by rare earth ion (La<sup>3+</sup>) in compositional-dependent borate glass, *Mater. Chem. Phys.* 289 (2022), 126503, <https://doi.org/10.1016/j.matchemphys.2022.126503>.
- [47] A.M. Babeer, A.E. Mahmoud, H.Y. Morshidy, Ligand field parameters, optical, thermal, magnetic, and structural features of ZnO containing cobalt-borate glasses, *Mater. Chem. Phys.* (2023), 143747, <https://doi.org/10.1016/j.matchemphys.2023.127681>.
- [48] M.S. Sadeq, H.Y. Morshidy, Effect of samarium oxide on structural, optical and electrical properties of some aluminoborate glasses with constant copper chloride, *J. Rare Earths* 38 (2020) 770–775.
- [49] M.I. Sayyed, A. Ibrahim, M.A. Abdo, M.S. Sadeq, The combination of high optical transparency and radiation shielding effectiveness of zinc sodium borate glasses by tungsten oxide additions, *J. Alloys Compd.* 904 (2022), 164037.
- [50] H. Ticha, L. Tichy, Semiempirical relation between non-linear susceptibility (refractive index), linear refractive index and optical gap and its application to amorphous chalcogenides, *J. Optoelectron. Adv. Mater.* 4 (2) (2002) 381–386.
- [51] I.S. Mahmoud, M.S. Gaafar, S.Y. Marzouk, Role of Sm<sup>3+</sup> ions on structural, optical and radiation shielding properties of lead borosilicate glasses, *J. Mater. Res. Technol.* 13 (2021) 1032–1044, <https://doi.org/10.1016/j.jmrt.2021.05.051>.
- [52] S. Stalin, D.K. Gaikwad, M.S. Al-buriah, C. Srinivasu, S. Amer, O. Tekin, S. Rahman, Influence of Bi<sup>2+</sup> O<sup>3</sup>/WO<sub>3</sub> substitution on the optical, mechanical, chemical durability and gamma ray shielding properties of lithium-borate glasses, *Ceram. Int.* 47 (2021) 5286–5299, <https://doi.org/10.1016/j.ceramint.2020.10.109>.
- [53] M.S. Sadeq, The tungsten oxide within phosphate glasses to investigate the structural, optical, and shielding properties variations, *J. Mater. Sci. Mater. Electron.* 32 (2021) 12402–12413, <https://doi.org/10.1007/s10854-021-05871-0>.
- [54] M.S. Sadeq, M.I. Sayyed, M.A. Abdo, H. Elhosiny Ali, H.A. Ahmed, Impact of lead oxide on the structure, optical, and radiation shielding properties of potassium borate glass doped with samarium ions M.I. Optik (2023), 170738, <https://doi.org/10.1016/j.jleo.2023.170738>.
- [55] A. Ibrahim, M.A. Farag, M.S. Sadeq, Towards highly transparent tungsten zinc sodium borate glasses for radiation shielding purposes, *Ceram. Int.* 48 (2022) 12079–12090.
- [56] W. Cheewasukhanont, P. Limkitjaroenporn, M.I. Sayyed, S. Kothan, H.J. Kim, High density of tungsten gadolinium borate glasses for radiation shielding material: effect of WO<sub>3</sub> concentration, *Radiat. Phys. Chem.* 192 (2022), 109926, <https://doi.org/10.1016/j.radphyschem.2021.109926>.
- [57] M.I. Sayyed, A.M. Abdel-Ghany, A. Askin, E.M. Sedqy, M.S. Sadeq, The structure, optical basicity, ligand field strength and shielding parameters of alkali/alkaline borate glasses doped with V<sub>2</sub>O<sub>5</sub>, *Opt. Mater.* 142 (2023), 114078.
- [58] M.I. Sayyed, M.S. Sadeq, Kh.S. Shaaban, A.F. Abd El-Rehim, Atif Mossad Ali, H. Y. Morshidy, Elucidating the effect of La<sub>2</sub>O<sub>3</sub>–B<sub>2</sub>O<sub>3</sub> exchange on structure, optical and radiation shielding improvements of Na<sub>2</sub>O–NiO–B<sub>2</sub>O<sub>3</sub> glass, *Opt. Mater.* 142 (2023), 114051.